Hindawi
Advances in Meteorology
Volume 2022, Article ID 6404243, 20 pages
https://doi.org/10.1155/2022/6404243

Research Article

Comparison of Multi-Satellite Precipitation Data from the Global Precipitation Measurement Mission and Tropical Rainfall Measurement Mission Datasets: Seasonal and Diurnal Cycles

Yilei Wang [1,2] **and Qiaoyan Wu** [1,2]

[1]*School of Oceanography, Shanghai Jiao Tong University, Shanghai 200030, China*
[2]*State Key Laboratory of Satellite Ocean Environment Dynamics, Second Institute of Oceanography, Ministry of Natural Resources, Hangzhou, Zhejiang 310012, China*

Correspondence should be addressed to Qiaoyan Wu; qwu@sio.org.cn

Received 26 August 2021; Revised 2 December 2021; Accepted 23 December 2021; Published 18 January 2022

Academic Editor: Stefania Bonafoni

A comparison was made between seasonal and diurnal variations in the Integrated Multi-Satellite Retrievals for Global Precipitation Measurement (IMERG) version 06B Final run and TRMM Multi-Satellite Precipitation Analysis (TMPA) 3B42 version 7 products from April 2014 to March 2019. As for earlier IMERG versions, systematic differences between IMERG version 06B precipitation and TMPA precipitation data were larger over the oceans than over land. Systematic annual mean differences between the IMERG and TMPA data over the oceans were smaller for IMERG version 06B than for earlier IMERG versions, possibly because of updated calibration processes. The mean differences between the IMERG version 06B and TMPA data for tropical oceans were relatively smtropical Pacific for all four seasons were not. The diurnal amplitudes of the IMERG were smaller than those of the TMPA over most continents, and the differences increased with mean diurnal amplitudes. The diurnal amplitudes of the IMERG were larger than those of the TMPA data over the oceans. The differences between the phases of the precipitation diurnal harmonics in the IMERG and TMPA datasets varied widely in all four seasons, but the mean phases were almost the same over both the oceans and the land. The sources of the differences in diurnal precipitation amplitudes in the Bay of Bengal and along the west coast of Central America, which showed large diurnal ranges and rather different diurnal amplitudes, were assessed. Differences in seasonal means caused differences in diurnal amplitudes in the Bay of Bengal, but for Central America, differences in diurnal amplitudes were associated with seasonal mean diurnal amplitudes.

1. Introduction

As an important element in the global hydrological cycle, precipitation affects clouds, water vapor, and the atmosphere through the exchange of latent heat, and it influences oceanic circulation through its effect on seawater salinity, as well as changing the surface reflectance by regulating the cryoconite cover [1–3]. Accurate measuring of precipitation is important for researches on the global energy balance. Satellite remote sensing precipitation products have been used commonly in climate studies and applications in recent decades. These satellite products are based mainly on microwave and infrared (IR) retrieval data [4–7]. Whereas most microwave sensors can provide precipitation data with a good degree of accuracy but poor coverage and low temporal resolution, IR sensors afford better coverage and temporal resolution but provide less accurate estimates of precipitation [4, 8, 9].

The Tropical Rainfall Measuring Mission (TRMM) dataset used to be one of the most widely used satellite remote sensing precipitation datasets in tropical hydrological studies. The TRMM Multi-Satellite Precipitation Analysis (TMPA) dataset uses precipitation estimates from multiple satellites as a calibration-based sequential scheme and provides estimates of precipitation at a finer resolution than former TRMM datasets [4, 10]. TRMM had operated

for 17 years from 1997 before being decommissioned on 15 April 2015. The Global Precipitation Measurement (GPM) mission, the successor to TRMM, was led by the Japanese Aerospace Exploration Agency (JAXA) and the US National Aeronautics and Space Administration (NASA) and was launched on 27 February 2014 [10, 11]. The Integrated Multi-Satellite Retrievals for GPM (IMERG) products provide estimates of precipitation with wider coverage, higher spatial and temporal resolution, and better snowfall estimates than TMPA products [12].

Despite improvements in satellite-based precipitation estimates, there are still some uncertainties in the data. Sampling errors (caused by the discrete revisit time and gaps in spatial cover) and retrieval errors (caused by the retrieval relationship between satellite observations and rain rates) are two important sources of error in precipitation estimates made using satellite data. Retrieval errors are different for different surface conditions, climate regions, and seasons, so different products perform differently for different areas [13]. The updated versions of IMERG generally perform better than older versions [14], but IMERG version 05 data have been found to be better than the latest IMERG version 06 data for certain regions [15].

Mean precipitation was estimated more accurately using IMERG than TMPA products in previous studies in which TMPA and IMERG daily or monthly products were compared [16–21]. However, the performances of IMERG and TMPA products at a diurnal scale have never been compared at a global scale. IMERG data prior to version 06 have been found to contain a lag compared with in situ rain gauge precipitation data over land and great uncertainty in precipitation amplitude, with the precipitation amount being represented better than the precipitation frequency and conditional precipitation rate [17, 22–25]. Intercalibration and interpolation were better in IMERG version 06 than in earlier versions [26], giving more confidence in the representation of the diurnal cycle by IMERG version 06 than by earlier versions. Tan et al. [27] compared diurnal cycles in the United States from IMERG V06 data and Multi-Radar Multi-Sensor ground observation data and found that the diurnal phases corresponded well but there were some disparities in diurnal amplitudes remained.

Over the last two decades, studies of the global precipitation diurnal cycle have been based mainly on TRMM data [28–32]. The TMPA 3B42 product from the TRMM data was used due to their high temporal and spatial resolution, and because the data were calibrated using rain gauges. It has been shown that for most regions, the TMPA 3B42 product captured the main diurnal variations in precipitation but was affected by some quantitative errors in diurnal phase and amplitude in some regions [33–39]. Comparisons of the TMPA and IMERG datasets with rain gauge data for Mainland China, Africa, and the Indian subcontinent indicate that diurnal variations may be estimated better using IMERG than TMPA [17, 19, 40]. Prakash et al. [41] compared the TMPA and IMERG datasets for the north Indian Ocean with data collected by ocean buoys at different timescales and found that the satellite observations performed better at the daily and monthly scales than at the diurnal scale.

Whilst satellite datasets have been evaluated in several previous studies, the performance of the latest GPM IMERG estimate (version 06B) against the previous TMPA products at the global scale needs to be investigated further, particularly at the diurnal scale. The main objectives of this study are (1) to compare the latest IMERG version 06B product with the TMPA 3B42 product to assess differences between the products at the seasonal and diurnal scales and (2) to attempt to identify the cause(s) of diurnal differences between the IMERG version 06B and the TMPA 3B42 product.

2. Materials and Methods

2.1. IMERG Data. The Final runs of the most recent version of the IMERG data (IMERG version 06B) were used. Precipitation estimates were provided at $0.1^\circ \times 0.1^\circ$ and 0.5 h resolutions covering 90° S–90° N (increased from 60° S–60° N in IMERG version 05). The IMERG algorithm combines microwave and IR sensor data and monthly gauge precipitation data from the whole of the GPM constellation [11]. The GPM core observatory satellite contains a dual-frequency precipitation radar and the GPM microwave imager [40]. The dual-band precipitation radar gives a better estimate of the sizes of precipitation particles and covers a wider range of precipitation rates than the single-band radar on the TRMM satellite [11]. It should be noted that some major changes were made in IMERG dataset when the data version updated from v05 to v06. The "displacement vectors" were computed using Modern-Era Retrospective Reanalysis 2 and Goddard Earth Observing System model forward processing data for version 06, but using IR data for version 05 [26, 42, 43]. Unlike the IMERG version 05 dataset, the version 06 dataset incorporated the Goddard profiling algorithm-TRMM microwave imager V05 estimates computed for the GPM era, and for the first time incorporated Sounder for Atmospheric Profiling of Humidity in the Intertropics by Radiometry estimates computed using the Precipitation Retrieval and Profiling Scheme [26]. A new morphing scheme based on total precipitable water vapor determined using numerical models was included in IMERG version 06. This was considered to be an improvement over the previous IR-based scheme, particularly for Southern Ocean latitudes [26]. There was less artificial variability in the diurnal cycle during times when only occasional samples were collected by nonSun-synchronous PMW satellites, such as the GPM microwave imager [42].

2.2. TMPA Data. The TMPA 3B42 (version 7) data product, with resolutions of $0.25^\circ \times 0.25^\circ$ and 3 h and a coverage of 50° S–50° N, was a post-real-time research-quality product released 3.5 months after the end of each month [4]. Microwave and IR sensors were used to estimate precipitation for TMPA datasets. The microwave radiometers were onboard the low Earth orbit platforms and operated at different frequencies, in which a TRMM microwave imager, a Special Sensor Microwave Imager/Sounder, an Advanced Microwave Scanning Radiometer for Earth Observing Systems, an Advanced Microwave Sounding Unit-B, and a

Microwave Humidity Sounder were included. IR data were collected by an international constellation of geosynchronous Earth orbit satellites [4, 12]. Four steps were involved in producing the TMPA dataset. First, the microwave precipitation estimates using the Goddard profiling algorithm were calibrated and combined to estimate precipitation rates. Second, the calibrated microwave estimates were used to calibrate the IR precipitation estimates. Third, IR estimates were used to fill gaps in the merged microwave datasets. Finally, the rain gauge data were combined with the multi-satellite data [4, 10].

2.3. Rain Gauge Data. The Global Tropical Moored Buoy Array (GTMBA) was designed as an *in situ* observing system over the tropical ocean by National Oceanic and Atmospheric Administration (NOAA) Pacific Marine Environmental Laboratory (PMEL) and the Joint Institute for the Study of the Atmosphere and Ocean (JISAO) [44]. The GTMBA included the Tropical Atmosphere–Ocean (TAO)/Triangle Trans-Ocean Buoy Network (TRITON) for the Pacific [45–47], the Pilot Research Moored Array in the Atlantic (PIRATA) for the Atlantic [47–49], and the Research Moored Array for African–Asian–Australian Monsoon Analysis and Prediction (RAMA) for the Indian Ocean [50]. Self-siphoning rain gauges were installed on the buoys and were calibrated at PMEL. Rain gauges are generally assumed to underestimate rainfall due to wind effects [47]. There were 2 TRITON buoys over the Pacific Ocean, 2 PIRATA buoys over the Atlantic Ocean, and 5 RAMA buoys over the Indian Ocean with one-hour resolution and more than one-year data available to compare diurnal variations with IMERG and TMPA data. The locations of these buoys were marked in Figure 1(a). The rain gauge data were averaged to 3-hourly resolution centred at 0000, 0300, 0600, 0900, 1200, 1500, 1800, and 2100 UTC as the intervals in TPMA data.

3. Methods

Seasonal and diurnal variations in the TMPA and IMERG datasets were compared for the complete 5-year period, from 1 April 2014 to 31 March 2019. TMPA data ceased to be available at the end of 2019. The TMPA and IMERG datasets have different spatial resolutions, so the data in each dataset were interpolated to $1^\circ \times 1^\circ$ grids using a linear interpolation method to allow comparison of seasonal and diurnal variations in the two precipitation products at the global scale. The temporal resolutions of the TMPA and IMERG data were 3 and 0.5 h, respectively, so there were 8 and 48 records at each grid point, respectively. Only diurnal variations were considered; semidiurnal variations were not taken into account. Based on climatological mean 3 h values from both datasets, the diurnal harmonics for each grid were calculated using the following equation [3, 51–53]:

$$p(t_i) = p_0 + \left[a_c \cos\left(\frac{2\pi t_i}{24}\right) + a_s \sin\left(\frac{2\pi t_i}{24}\right)\right] + \varepsilon_i, \quad (1)$$

where p is the precipitation estimate at time t_i in the dataset of interest, $t_i = 0, 3, \ldots, 21$ are times at 3 h intervals, p_0 is the daily mean precipitation for the 5-year period for each grid, a_c and a_s are the cosine and sine component coefficients in the Fourier representation of the precipitation estimates, and ε_i is the residual. The amplitude $A = \sqrt{{a_c}^2 + {a_s}^2}$ and phase $\phi = \arctan(a_s/a_c)$ were calculated using this function. The time of the maximum in the diurnal cycle was determined as the phase ϕ. Estimates made using the TMPA and IMERG datasets were adjusted to local solar time for each degree of longitude on the grid. *F*-tests were performed to assess the harmonics for statistical significance to make sure that the harmonic features were significant [54]. Diurnal harmonics in IMERG precipitation were calculated using both the 0.5 and 3 h values averaged from the 0.5 h data. The 3 h values data were centred at 0000, 0300, 0600, 0900, 1200, 1500, 1800, and 2100 UTC to match the intervals in TPMA data.

4. Results and Discussion

The 5-year (from April 2014 to March 2019) mean precipitation data from the IMERG dataset are shown in Figure 1(a). The IMERG product captured the regions with heavy precipitation, including the Pacific and Atlantic intertropical convergence zones (ITCZs), the Pacific warm pool, the South Pacific convergence zone (SPCZ), and the Indian Ocean. Heavy precipitation was also found for the Kuroshio Extension and the Gulf Stream regions. The differences and relative differences between the IMERG and TMPA precipitation data (IMERG minus TMPA and IMERG minus TMPA relative to the IMERG 5-year mean, respectively) for the 5-year period are shown in Figures 1(b) and 1(c), respectively. Rainfall at latitudes higher than 25°S or 25°N over the ocean was higher in the IMERG product than in the TMPA product. The differences between the IMERG and TMPA rainfall data for the tropical oceans were <1 mm/d except for the Atlantic ITCZ, for which the IMERG dataset inticated relatively low rainfall. Rainfall over the oceans was higher in the IMERG than in the TMPA product at low rates of rainfall, but the differences between the IMERG and TMPA products were small at high rainfall. The relative differences between the IMERG and TMPA precipitation data followed a similar pattern to the differences between IMERG and TMPA precipitation data, except for some dry regions in the southern Pacific and southern Atlantic.

The mean systematic differences between the precipitation data in IMERG version 06B and TMPA version 7 over the ocean between April 2014 and March 2019 are shown in Figure 1(b), which were distinct from the mean precipitation differences between the previous IMERG version and TMPA version 7 [21]. Rainfall was lower in the IMERG version 05 data than the TMPA version 7 data for all the tropical oceans between 1 April 2014 and 30 April 2017, and the IMERG rainfall data were much lower than the TMPA rainfall data for high-rainfall areas in the tropics [21]. Regarding the differences between the IMERG version 03D data and TMPA version 7 data for the first year of the GPM, as shown in [16], the pattern

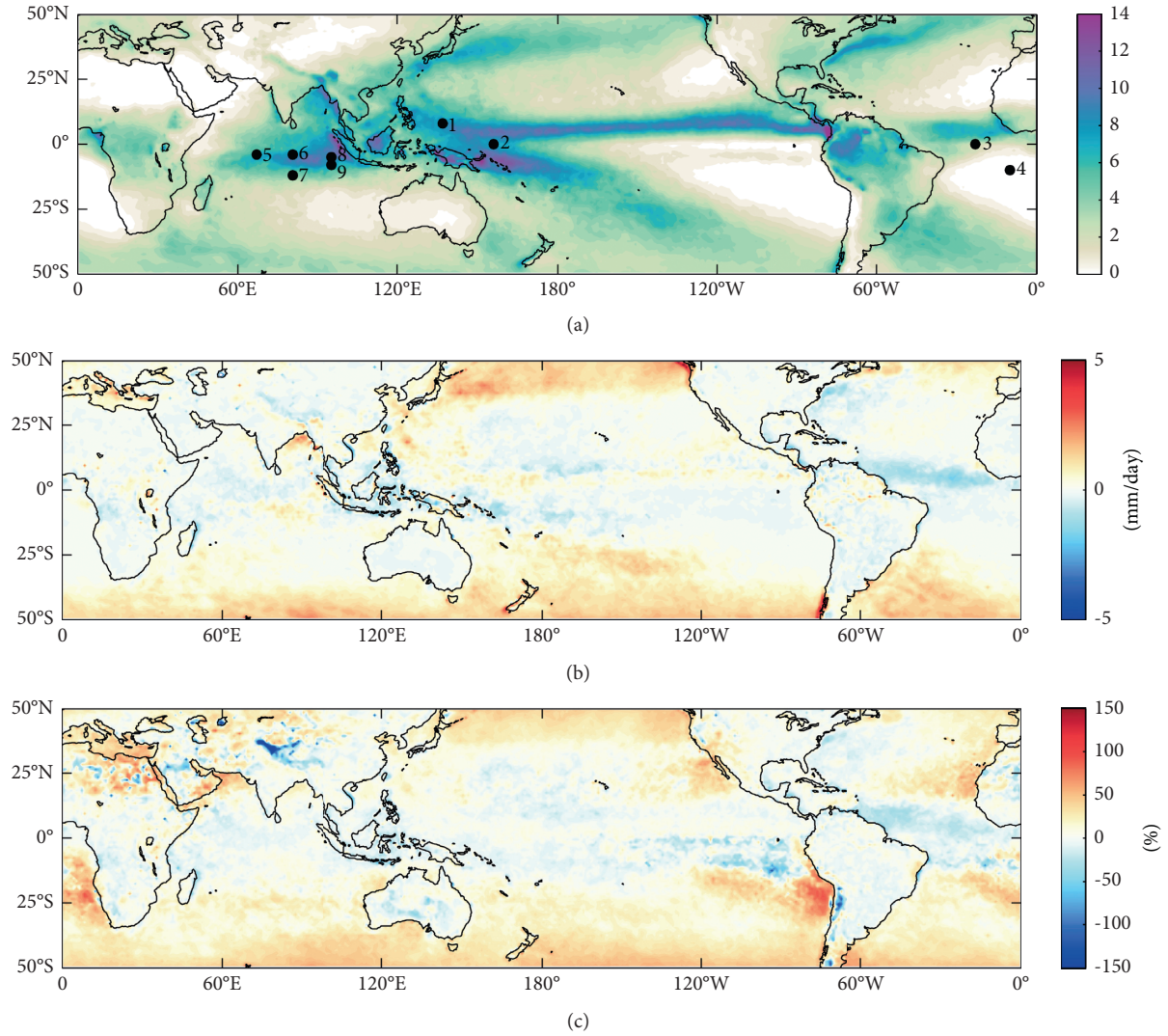

Figure 1: Climatological mean precipitations. (a) Five-year mean precipitation data from the IMERG V06B product. The positions of nine ocean buoys were marked; (b) mean differences (IMERG minus TMPA); (c) relative differences (IMERG minus TMPA, relative to the IMERG mean).

was similar to that seen in the mean systematic differences between the IMERG version 05 and TMPA data. The different patterns in the differences between IMERG version 06 and TMPA precipitation data and the previous IMERG version data reflected differences between the annual mean data in IMERG version 06 and earlier IMERG versions [16, 21], which could have been caused by updated calibration processes used in IMERG version 06. For the IMERG version 06 estimates, TRMM-based calibrations were performed in the first 2.5 months of the GPM era and the GPM-based calibrations were then performed in the remaining part, whereas for IMERG version 05 and other earlier versions, the GPM-based calibrations were used in the whole period [26]. The differences between the data from the various IMERG versions and the TMPA data were much smaller over land than over ocean because the IMERG and TMPA datasets were all produced using Global Precipitation Climatology Centre (GPCC) gauge adjustments to correct bias over land.

4.1. Comparison of Seasonal Cycles in the IMERG and TMPA Datasets. Differences in mean precipitation seen in the datasets from the IMERG and TMPA products in different seasons are shown in Figure 2. The figure was prepared to determine whether any differences in patterns between the IMERG and TMPA products were consistent for all seasons. It is interesting to note that although the differences between the IMERG and TMPA 5-year mean precipitation data for the tropical oceans were generally small, the differences for all seasons in the tropical Pacific were considerable. Rainfall in the Pacific ITCZ was higher in the IMERG product than in the TMPA product in the boreal spring, but lower in the boreal summer. Rainfall in the SPCZ was lower in the IMERG products than the TMPA products for the boreal spring, summer, and autumn but higher in the IMERG products than the TMPA products for the boreal winter. The fact that the differences were opposite in different seasons meant that the IMERG and TMPA 5-year mean differences

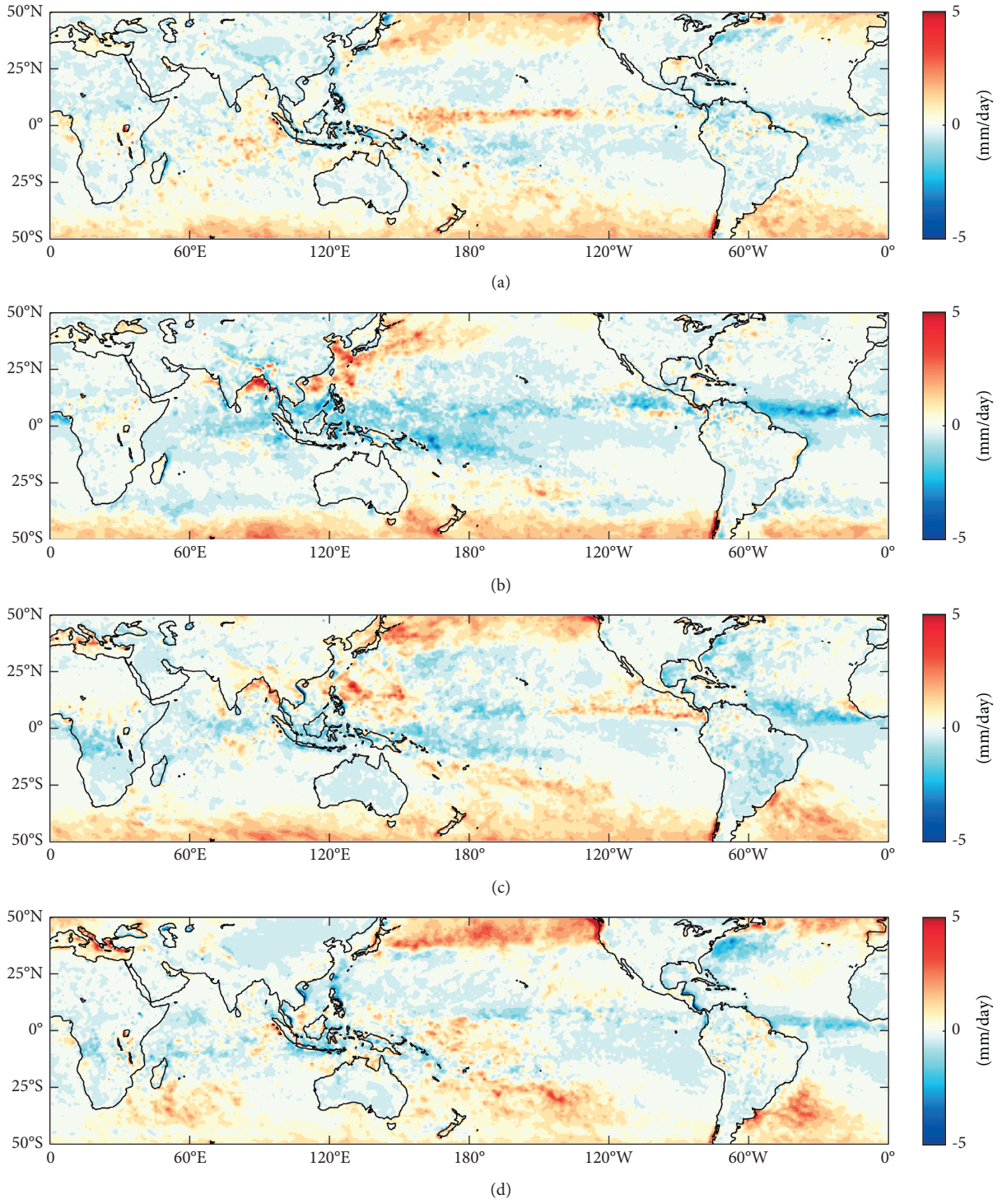

Figure 2: Differences (IMERG minus TMPA) between the mean precipitation data in the IMERG V06B product and the TMPA 3B42 product in (a) March, April, and May (MAM); (b) June, July, and August (JJA); (c) September, October, and November (SON); (d) December, January, and February (DJF).

for the tropical Pacific were small. Rainfall in the Atlantic ITCZ was lower in the IMERG dataset than the TMPA dataset in all seasons, and the largest difference was ~2 mm/d in the boreal summer. More rainfall at latitudes between 35°S and 50°S over the global oceans was found in the IMERG dataset than the TMPA dataset for all seasons. More rainfall over the Pacific Ocean between latitudes 35°N and 50°N in the boreal spring, autumn, and winter was observed from the IMERG dataset than from the TMPA dataset. The differences between the IMERG and TMPA datasets in all seasons were more consistent over land than over ocean (the differences over the land were <1 mm/d). Rainfall in high-

rainfall areas in the tropics was much lower in the IMERG version 03 data than in the TMPA version 7 data for the boreal summer 2014 and boreal winter 2014/2015 [16], suggesting possible seasonal mean differences between IMERG version 06 and its earlier version over ocean.

The TMPA and IMERG data showed differences over land and ocean in different seasons. Scatter plots of mean precipitation from the IMERG and TMPA data over land (red dots) and ocean (blue dots) in all four seasons are shown in Figure 3. Here, we roughly included both big islands and the maritime continent as land, and small islands smaller than $1^\circ \times 1^\circ$ as ocean areas. Spring was defined as March, April, and May (MAM) in the boreal hemisphere and September, October, and November (SON) in the austral hemisphere, and summer was defined as June, July, and August (JJA) in the boreal hemisphere and December, January, and February (DJF) in the austral hemisphere. Autumn was defined as SON in the boreal hemisphere and MAM in the austral hemisphere. Winter was defined as DJF in the boreal hemisphere and JJA in the austral hemisphere. In Figure 3, the dashed lines indicate one-to-one relationships. Lines were fitted to the data using the least-squares method. The IMERG products showed good correlation with the TMPA products over both ocean and land in all four seasons. The correlation coefficients were higher for the summer than the winter over the oceans and over the land. This indicates that the satellite datasets were more consistent in the summer than winter, which resulted from the different capacities of the satellite channels and associated algorithms to detect light precipitation. The intercepts of the lines fitted to the relationships between the IMERG and TMPA data were positive, and the slopes were close to 1 over both the oceans and the land for all four seasons. The intercepts were higher over the oceans compared to the land, indicating that IMERG estimated higher precipitation than the TMPA over ocean. The root mean squared errors between the datasets were smaller over land than over ocean for all four seasons. This is probably because the same GPCC gauge adjustment was applied to both datasets over land.

The relative differences between the satellite products for all four seasons are shown in Figure 4. Overall, regions with large relative differences were associated with scarce rainfall. The regions showing maximum relative differences over land were the Himalayas and Tibetan Plateau regions in DJF and MAM. Despite the same ground adjustment in two satellite datasets, the relative differences were still significant in this area. Xu et al. [18] compared the rainfall from the IMERG V03 and the TMPA 3B42 with gauges over the Tibetan Plateau and found that the TMPA had larger false alarm ratio while the IMERG had larger missing ratio. The negative relative differences indicate the better capability of the IMERG in measuring the light precipitation. Unlike for the differences shown in Figure 2, the relative differences between the satellite products were smaller for the tropical Pacific than for the other regions due to the high mean precipitation rate. Much lower rainfall in the Atlantic ITCZ was indicated in the IMERG dataset than the TMPA dataset in all four seasons (Figure 2), but the relative differences for the tropical Atlantic were inconsistent in all four seasons. Negative relative differences were found for the equatorial Atlantic in the boreal summer and autumn, and positive relative differences were found for the North Atlantic in the boreal spring and winter. Similar to the differences between the IMERG version 03 products and TMPA version 7 products for the boreal summer of 2014 and boreal winter of 2014/2015, the relative differences between the IMERG version 03 products and the TMPA version 7 products for the boreal summer of 2014 and the boreal winter of 2014/2015 [16] were very different from the relative differences between the IMERG version 06 products and the TMPA version 7 products as shown in Figures 4(b) and 4(d).

The differences between the IMERG version 06 and TMPA version 7 products over land were relatively small for all seasons, but the relative differences were quite large for some regions. Large relative differences were mostly found for low precipitation regions over ocean and land. Less light precipitation was indicated in all of these dry regions by the IMERG estimates than by the TMPA estimates. For example, the relative differences between the IMERG and TMPA products reached −150% over Asia in the boreal winter.

4.2. Comparison of the Diurnal Cycles in the IMERG and TMPA Datasets. The amplitudes of the diurnal harmonics estimated from the seasonal mean IMERG datasets for the $1^\circ \times 1^\circ$ grid are shown in Figure 5. The harmonics that were not statistically significant at the 90% confidence level were masked with grey. These harmonics corresponded mostly to regions with little precipitation. The distributions of the amplitudes in the different seasons resembled the seasonal mean precipitation rates in the different seasons, with the diurnal amplitudes being larger in regions with higher mean precipitation rates, such as the ITCZ and maritime continental areas. The diurnal cycles of precipitation varied seasonally. Larger diurnal amplitudes were found over the continents in the northern hemisphere in the boreal summer and the southern hemisphere in the boreal winter. Larger diurnal amplitudes in precipitation over the ocean in the Bay of Bengal were found in the boreal summer than in other seasons. Diurnal variations in precipitation over the Gulf Stream were found only in the boreal summer. The diurnal variations in precipitation in Central America and the adjacent ocean were larger in the boreal summer and autumn than in the boreal winter and spring. The largest mean diurnal variations in precipitation were found over the tropical ocean due to deep convection, but marked diurnal differences were also found over areas of ocean with lower mean precipitation, including the ocean around the Indonesian islands, over the northern part of the Bay of Bengal, and along the Central American and Mexican coasts in JJA. The large diurnal amplitudes in these areas were considered to spread from convective regions over land to the adjacent oceans through complex land–sea breeze systems [55]. It is worth noting that the diurnal harmonics estimated from the seasonal mean IMERG datasets for the $1^\circ \times 1^\circ$ grid did not have statistical significance in most areas. It is possible that a longer record might stabilize the diurnal cycle and provide significance in areas that lack it in such a short record.

The differences between the amplitudes of the diurnal harmonics from the precipitation products (IMERG minus

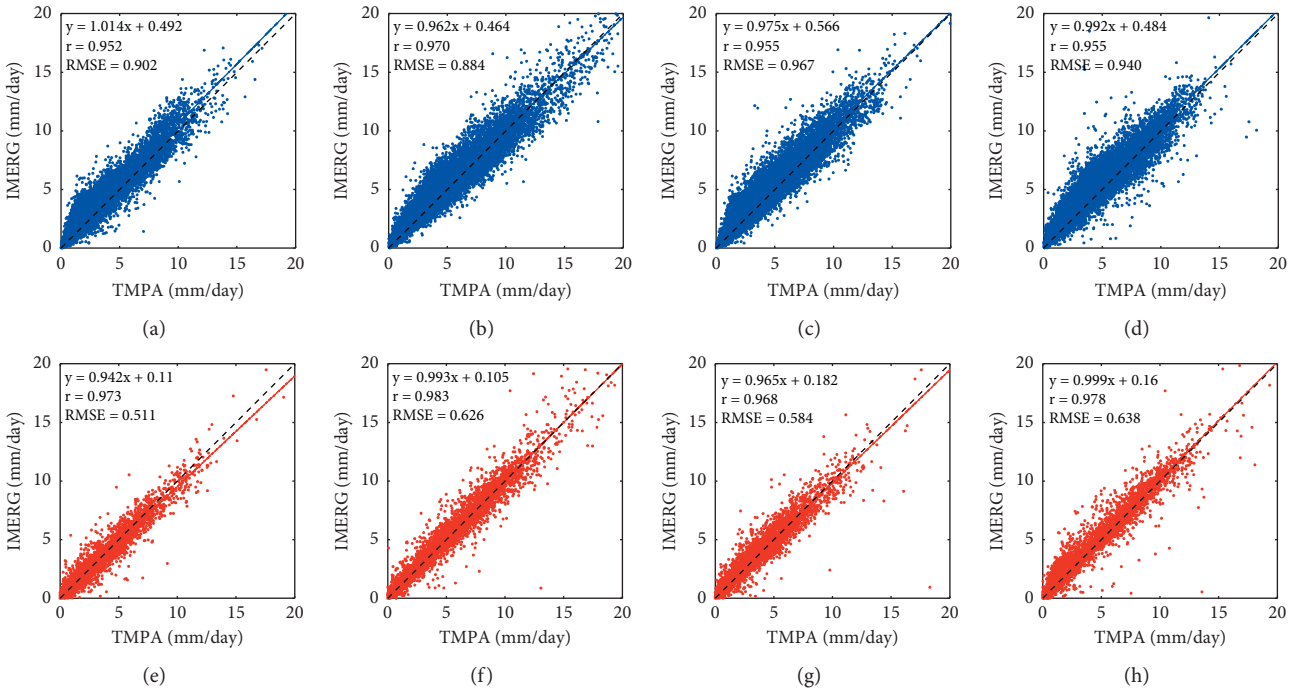

Figure 3: Scatter plots of seasonal mean precipitation in the IMERG V06B and TMPA 3B42 products over ocean (blue) and land (red) using a $1^{\circ} \times 1^{\circ}$ grids for (a, e) spring; (b, f) summer; (c, g) autumn; and (d, h) winter. The black dashed line indicates a one-to-one relationship.

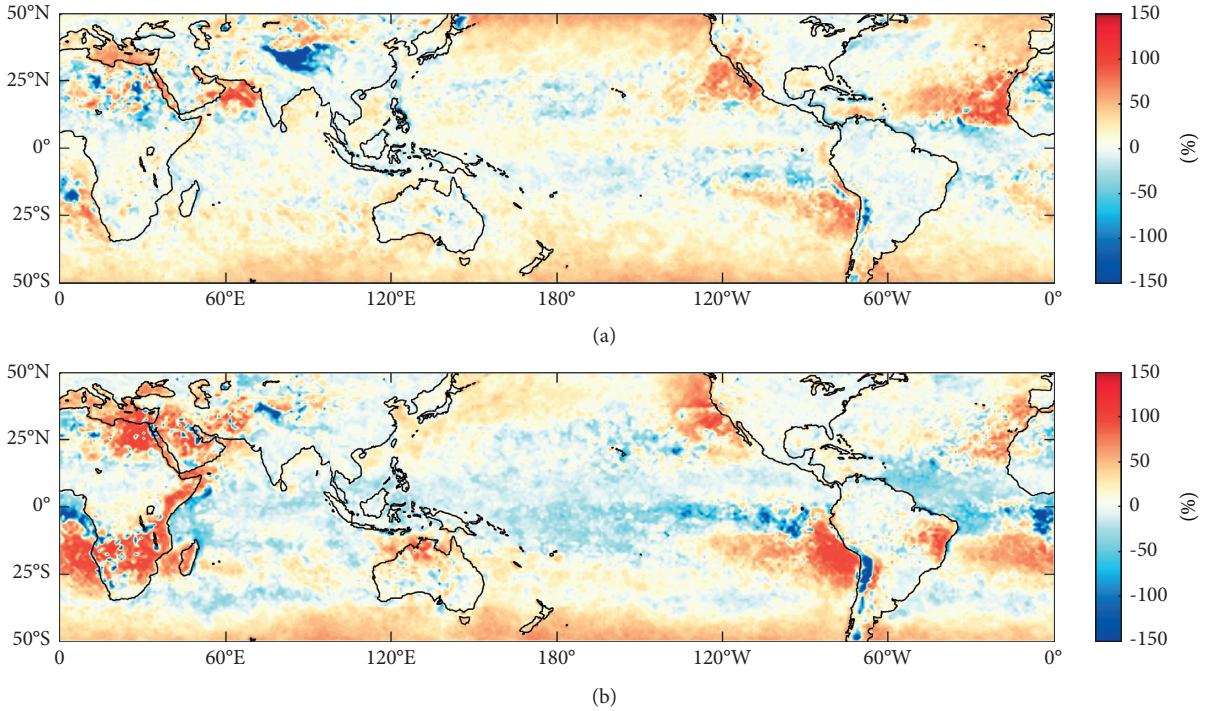

Figure 4: Continued.

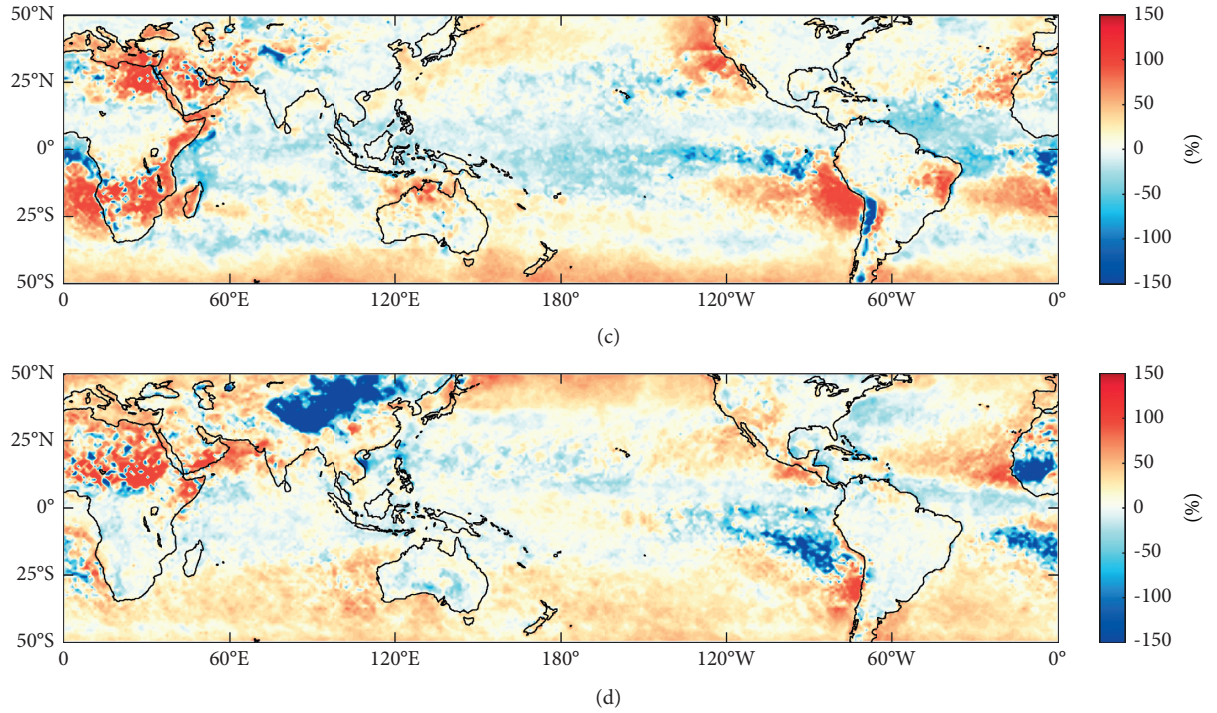

Figure 4: Relative differences (IMERG minus TMPA, relative to 5-year IMERG mean) between the IMERG V06B product and TMPA 3B42 product in (a) MAM; (b) JJA; (c) SON; and (d) DJF.

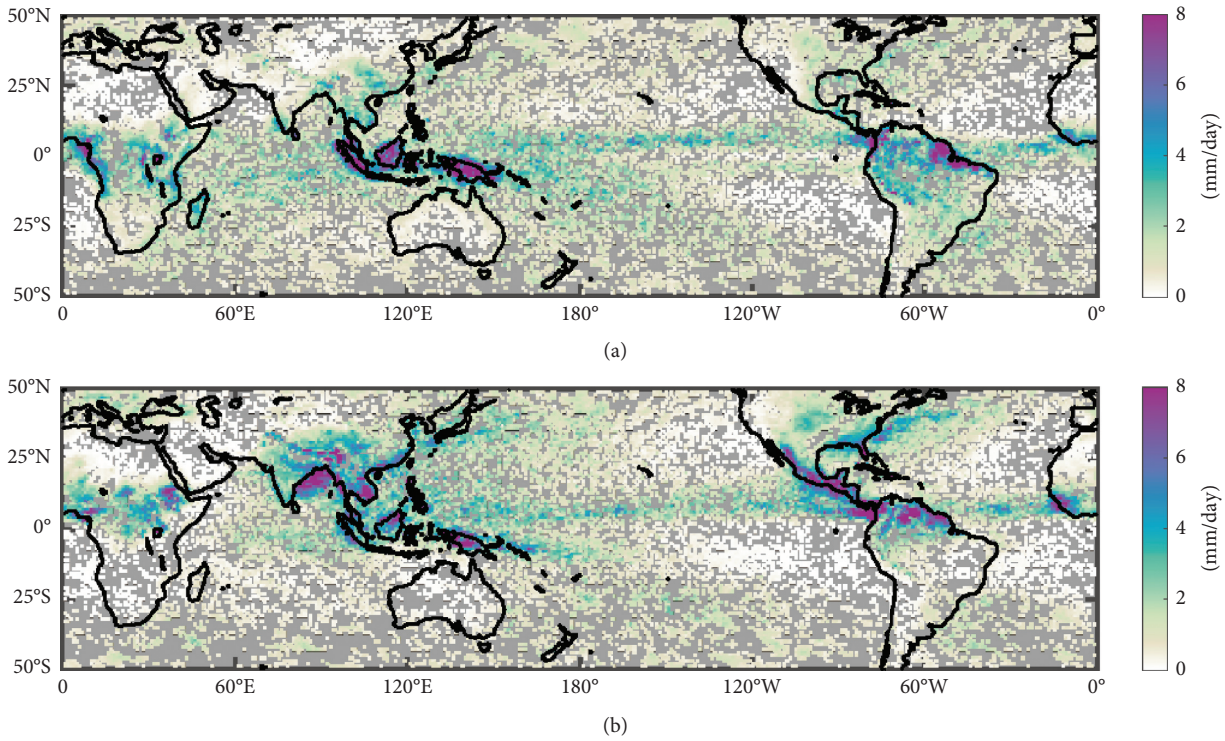

Figure 5: Continued.

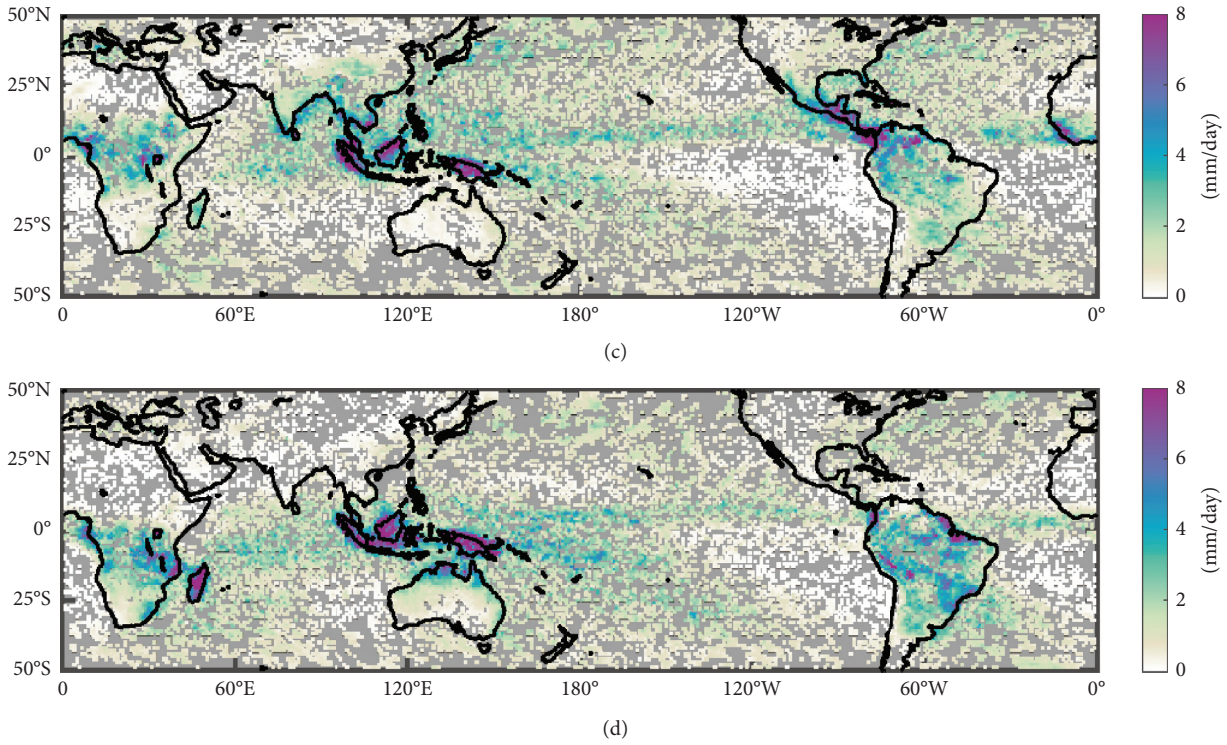

Figure 5: Amplitude of the diurnal harmonic from the IMERG V06B product in (a) MAM; (b) JJA; (c) SON; and (d) DJF. The grey shadowing represents that the diurnal harmonics were not statistically significant at the 90% confidence level.

TMPA) for the $1^\circ \times 1^\circ$ grid are shown in Figure 6. Comparisons were made at grid points at which the diurnal harmonics were significant at the 90% confidence level for both the IMERG and TMPA products. Unlike the seasonal mean differences, the diurnal differences in amplitude over land were not small. The diurnal variations over most of the continents and maritime continents were smaller for the IMERG data than for the TMPA data. The differences were the largest in high-rainfall regions in South America and Africa in SON and DJF. Over the oceans, larger diurnal variations were found in the IMERG data than in the TMPA data. Large positive diurnal differences were found in regions with large diurnal variations, such as the ITCZ in MAM and over the northern Bay of Bengal in JJA (Figure 5(b)). Large positive diurnal differences were also found in regions with relatively small diurnal variations, and small positive diurnal differences were found in regions with relatively large diurnal variations. This indicates that large diurnal differences between the IMERG and TMPA data were not necessarily associated with large diurnal variations. The distribution of diurnal mean differences did not resemble the pattern of seasonal mean difference over either ocean or land in any season, suggesting that the diurnal mean differences between the IMERG and TMPA data for most regions were not associated with the seasonal mean differences.

Scatter plots of the amplitudes of the IMERG and TMPA data over land and ocean in different seasons for the $1^\circ \times 1^\circ$ grid are shown in Figure 7. Dashed lines indicate one-to-one relationships, as in Figure 3. Lines were fitted to the data using the least-squares method. The diurnal amplitudes in the IMERG and TMPA data were well correlated over both the oceans and the land in all seasons. The intercepts for the lines fitted to the relationships between the diurnal amplitudes in the IMERG and TMPA products were between 0.242 and 0.314 mm/d over the oceans and close to zero over land. The slopes of the lines fitted to the relationships between the diurnal amplitudes in the IMERG and TMPA data were <1 over ocean and land but were closer to 1 over the oceans than over land. The intercepts and slopes indicate that the diurnal amplitudes over most of the ocean regions in all four seasons were larger in the IMERG data than in the TMPA data, because the diurnal amplitudes were <4 mm/d in most regions (Figure 5). The diurnal amplitudes over land in all four seasons were smaller in the IMERG data than in the TMPA data. The slopes were <1 and the intercepts were close to zero over land, so the differences between the diurnal amplitudes in the IMERG and TMPA datasets increased with the mean diurnal amplitudes. The correlation coefficients were higher over land than over ocean in all four seasons. The root mean squared differences between the diurnal amplitudes over both ocean and land in the IMERG and TMPA datasets were smallest in winter and largest in summer.

The distributions of the estimated phase of the diurnal harmonics of precipitation from the IMERG product for the $1^\circ \times 1^\circ$ grid for four seasons are shown in Figure 8. The diurnal harmonic phase represented the maximum precipitation time. The main characteristics of the diurnal precipitation cycle as indicated by the IMERG product were

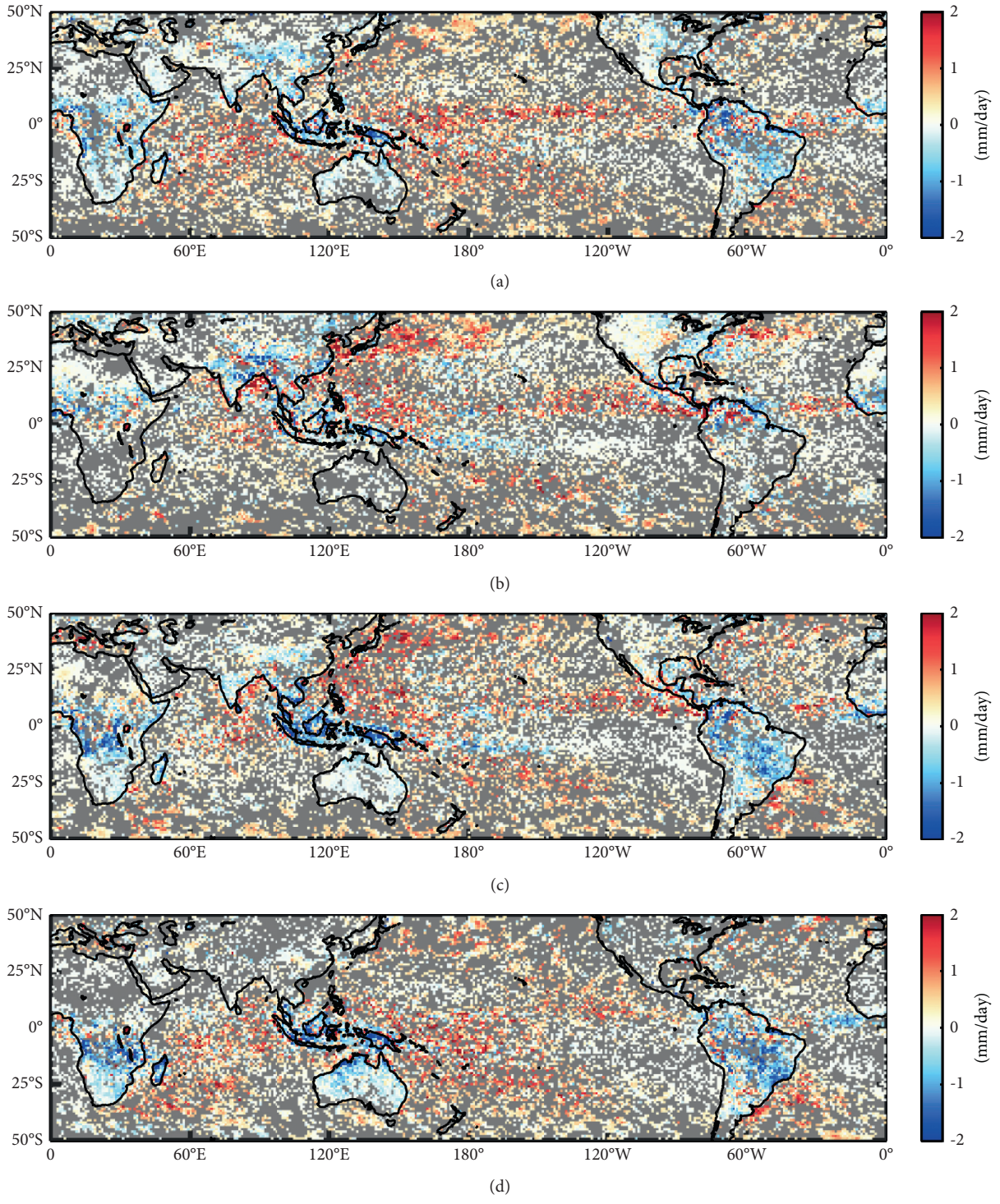

Figure 6: Differences (IMERG V06B minus TMPA 3B42) between the amplitude of the diurnal harmonics in (a) MAM; (b) JJA; (c) SON; and (d) DJF. The grey areas indicate where the diurnal harmonics were not statistically significant at the 90% confidence level in either IMERG or TMPA data.

that maximum precipitation over the tropical oceans occurred in the morning, and maximum precipitation over most of the land occurred in the late afternoon in all seasons. Maximum precipitation over land tended to occur around 1800 local time. The time of maximum diurnal precipitation could be affected by local topography in some regions. For example, the plains in the central United States, between the Rockies and the Appalachian Mountains, had maximum precipitation between midnight and early morning in JJA [56], and the regions near the Andes had maximum precipitation between midnight and early morning in DJF [57]. The patterns also varied as the seasons changed. In the boreal

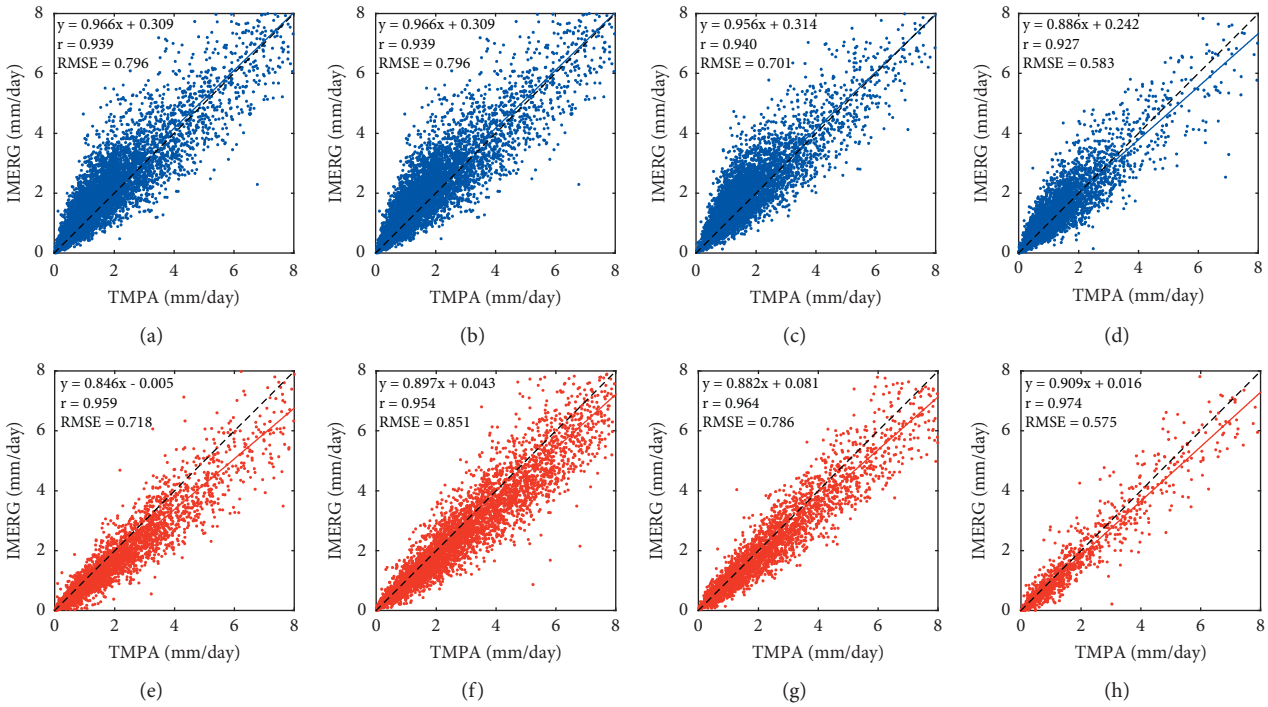

Figure 7: Scatter plots of the amplitude of the diurnal harmonics in the IMERG V06B and TMPA 3B42 products over ocean (blue) and land (red) using a $1^{\circ} \times 1^{\circ}$ grids for (a, e) spring; (b, f) summer; (c, g) autumn; and (d, h) winter. The black dashed line indicates a one-to-one relationship.

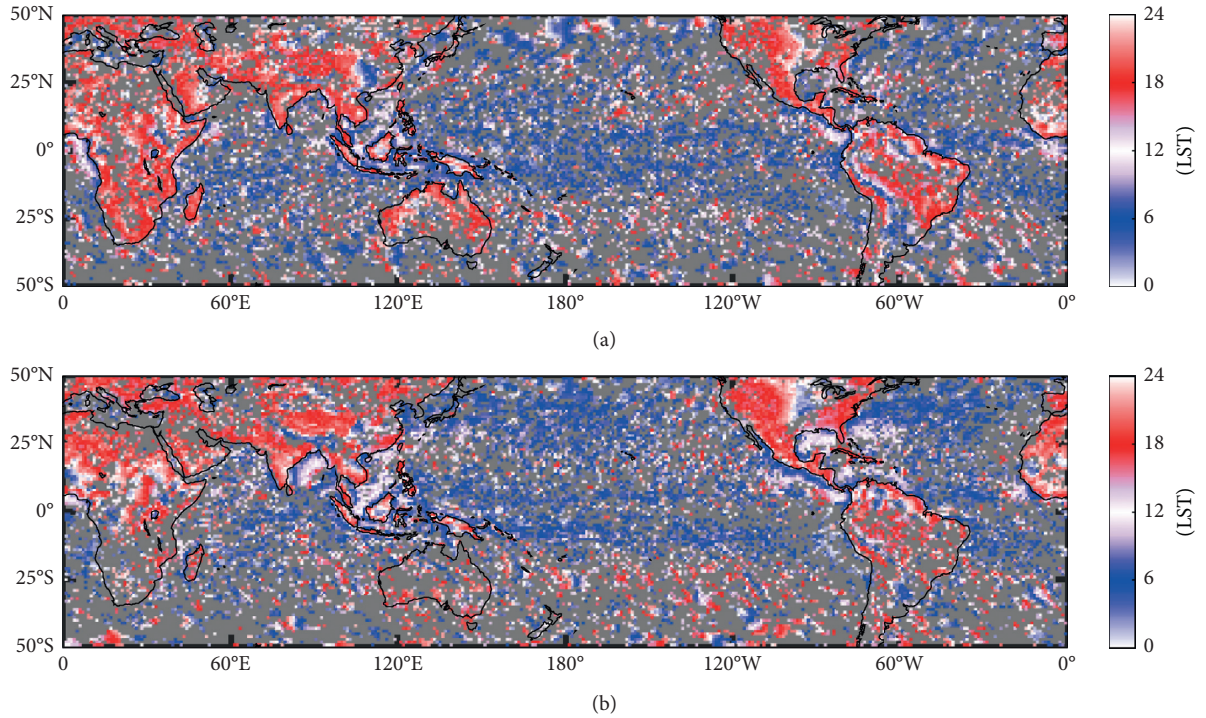

Figure 8: Continued.

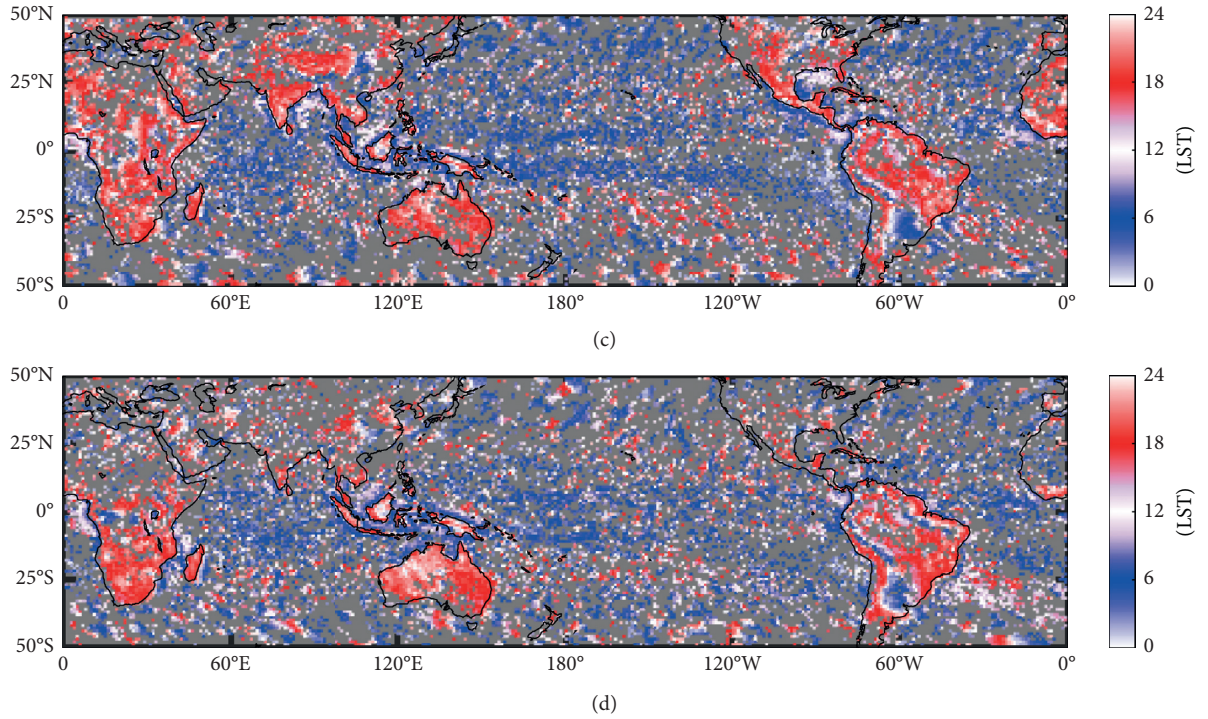

Figure 8: Peak time of the diurnal harmonics from the IMERG V06B product in (a) MAM; (b) JJA; (c) SON; and (d) DJF. The grey areas indicate the diurnal harmonics were not statistically significant at the 90% confidence level in either IMERG or TMPA data.

summer, the land–sea difference in maximum precipitation time was more marked in the northern hemisphere than in the southern hemisphere, and the opposite was found for the boreal winter. The time at which maximum precipitation occurred was much more variable over ocean than over land. In regions dominated by deep convection, such as the ITCZ and SPCZ, maximum precipitation occurred in the early morning (about 0600 local time). Noisier diurnal cycles were found over ocean than over land because only deep and organized convection tended to give an early morning maximum, but submesoscale convection (typical of suppressed conditions) tended to produce a late afternoon maximum much more similar to the case for land-based convection [58].

There were no clear patterns in the differences between the phases of the precipitation diurnal harmonics in the IMERG and TMPA datasets (figure not shown). The probability density functions of the differences in the times of the maxima in the diurnal harmonics in the IMERG and TMPA datasets using the $1^\circ \times 1^\circ$ grid over land and ocean in each season are shown in Figure 9. Overall, the phases in the IMERG and TMPA datasets were more consistent over land than over ocean except in the winter, when the differences in the phases in the diurnal harmonics showed similar probability density functions over land and ocean. The differences in the phases of the precipitation diurnal harmonics between the IMERG and TMPA datasets varied widely in all seasons, but the mean phases over both ocean and land were almost the same for the IMERG and TMPA datasets, except that the mean maximum time was ~0.5 h earlier in the TMPA dataset than in the IMERG dataset in both summer and winter over land, and the mean maximum time was ~0.5 h earlier in the IMERG dataset than in the TMPA dataset in autumn over ocean. It is worth noting that the diurnal cycles in the 3 h IMERG and 3 h averaged TMPA datasets were also compared. No significant differences were found between the 0.5 and 3 h averaged diurnal harmonics in the IMERG dataset.

4.3. Different Sources Cause Significant. Differences in Diurnal Amplitudes in the IMERG and TMPA Datasets, Using Two Regions as Examples

All the satellite data and most of the rain gauges detected diurnal signal peaking in the early morning in a statistically significant way. Overall, both satellite datasets showed similar diurnal variations as buoy measurements, except for Buoy 2, Buoy 4, and Buoy 6. Buoy 2 detected an evident semidiurnal cycle; however, semidiurnal cycles were not evident in either satellite datasets. For buoy 4 in the Atlantic Ocean and buoy 6 in the Indian Ocean, a significant peak at about 1400 LST had been found in the precipitation, while a morning peak was shown in both the IMERG and TMPA. The diurnal difference between gauges and satellite datasets could arise because the satellite datasets were $5^\circ \times 5^\circ$ area-averaged. A weaker and shallower afternoon peak over the oceans had been found in the earlier studies using either in situ or satellite measurements [13, 28, 55, 58, 59]. The morning peak was considered as a result of both stratiform and convective from deep clouds while the afternoon peak was only related to convective rainfall from midlevel clouds [58, 60].

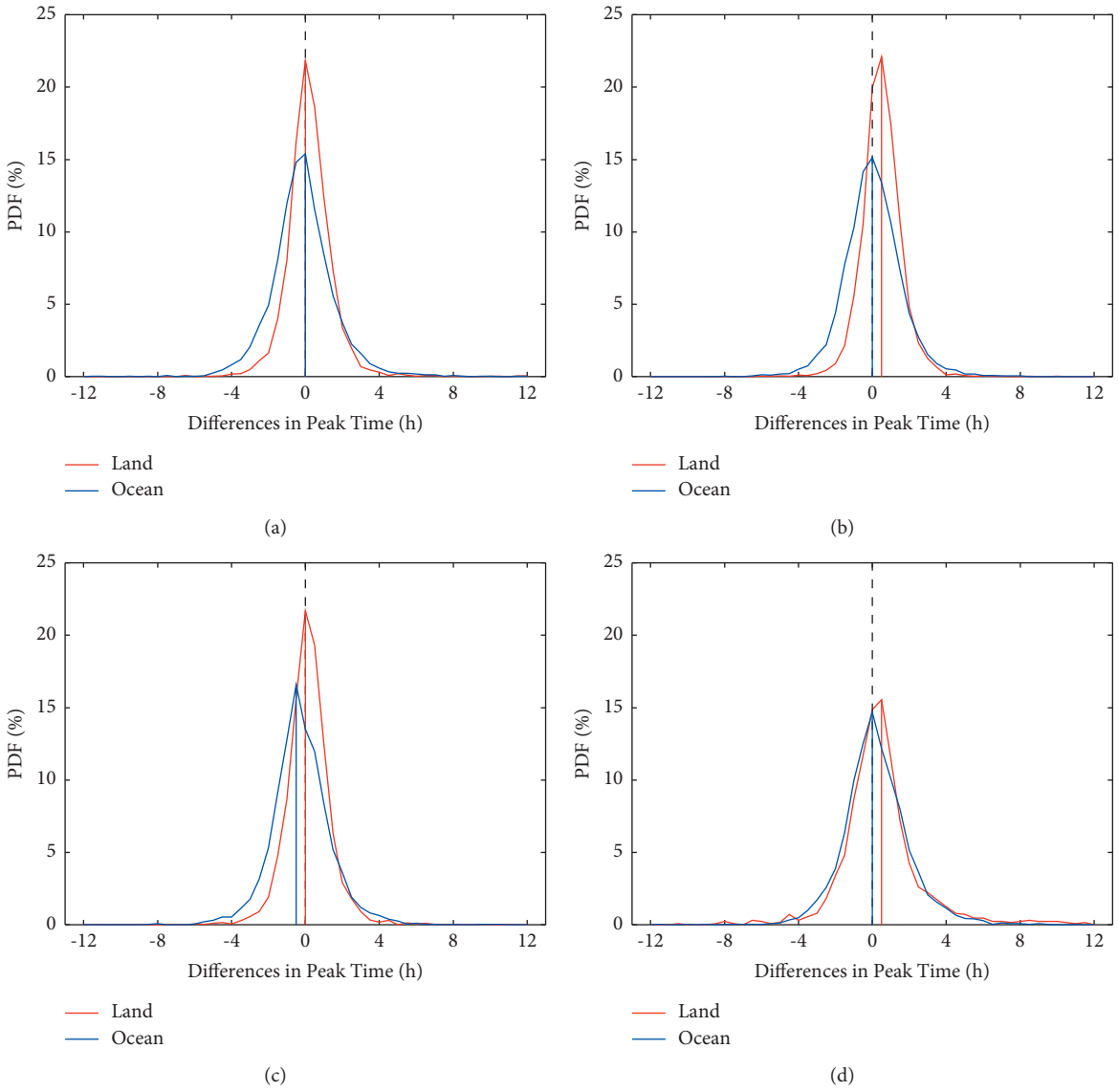

FIGURE 9: Probably density functions for the differences between the maximum times of the diurnal harmonics in the IMERG V06B product and TMPA 3B42 product in (a) spring; (b) summer; (c) autumn; and (d) winter.

It was shown in Section 4.2 that smaller diurnal variations over most of the continents and maritime continents were found in the IMERG dataset than in the TMPA dataset, and that the differences in the diurnal amplitudes over land in the IMERG and TMPA datasets increased with the mean diurnal amplitude. Diurnal variations over ocean were larger in the IMERG dataset than in the TMPA dataset, but the differences in the diurnal amplitudes in the IMERG and TMPA datasets were not necessarily associated with large diurnal amplitudes. The diurnal amplitudes in the different seasons were estimated from seasonal mean precipitation data. The large differences in the diurnal amplitudes in the IMERG and TMPA datasets may therefore have been caused by large seasonal mean differences or large diurnal amplitudes. Precipitation for the Bay of Bengal and the west coast of Central America, which showed large diurnal ranges and significant differences between the diurnal amplitudes in the IMERG and TMPA datasets, is presented here in detail as examples.

The diurnal amplitudes in the IMERG data, the seasonal mean differences between the IMERG and TMPA data, and the differences between the IMERG and TMPA diurnal amplitudes for the Bay of Bengal and the adjacent continents in JJA and DJF are shown in Figure 10. The northern Bay of Bengal and the east coast of the Bay of Bengal showed seasonal mean diurnal amplitudes >8 mm/d in JJA (Figure 10(a)). The amplitude was larger over the ocean than over most of the adjacent continental regions. The diurnal amplitudes in the northwest part of the Bay of Bengal were up to 2 mm/d larger in the IMERG data than in the TMPA data, but the diurnal amplitudes for the east coast of the Bay of Bengal were up to 2 mm/d smaller in the IMERG data than in the TMPA data (Figure 10(b)). However, the seasonal mean diurnal amplitudes were large in both areas. The seasonal mean differences between the IMERG and TMPA data are shown in Figure 10(c). The patterns in the seasonal mean differences were similar to the patterns in the diurnal

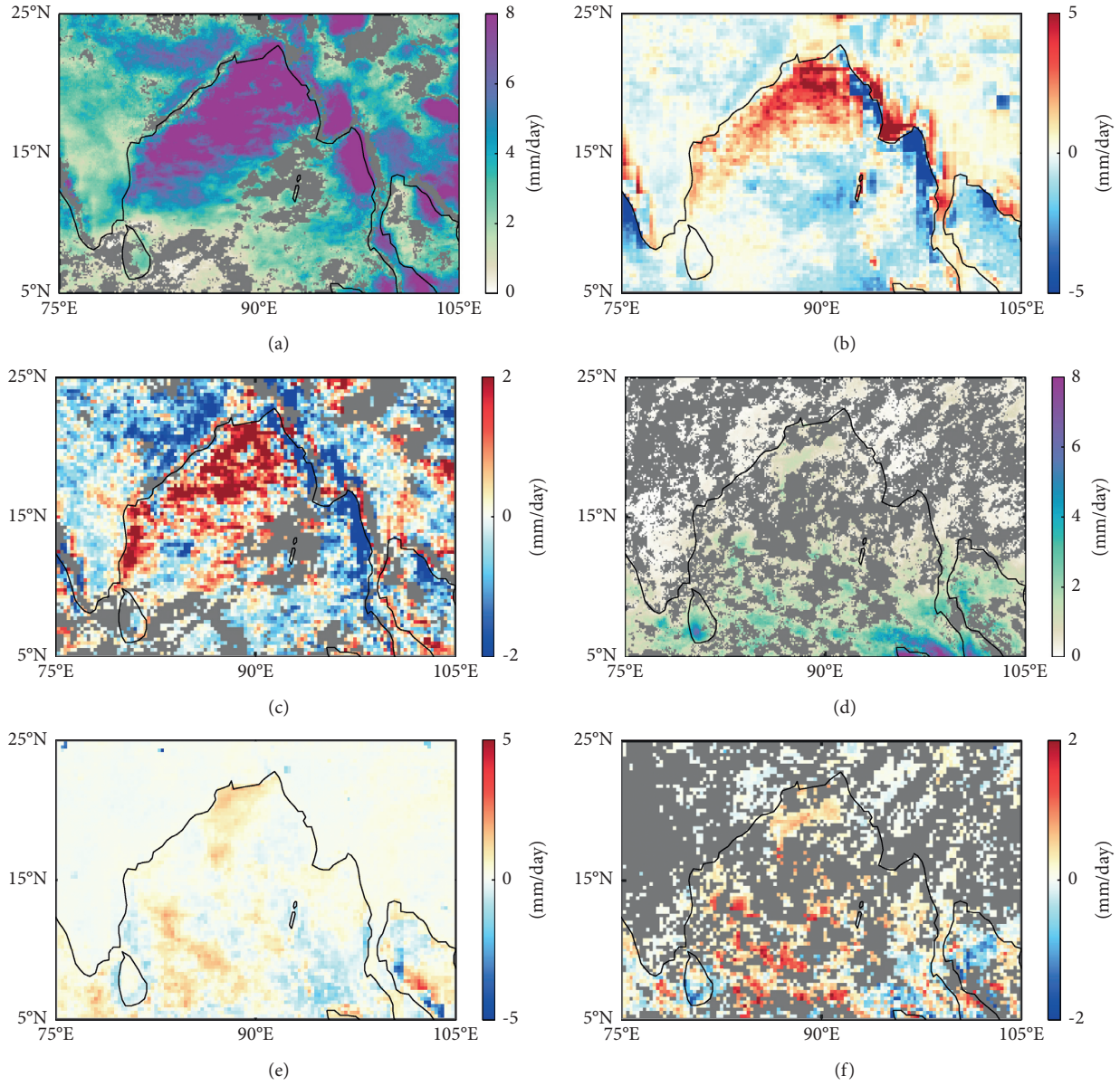

Figure 10: Amplitudes of the diurnal cycles in the IMERG data, differences between mean precipitation, and differences between mean precipitation diurnal amplitude in the IMERG V06B and TMPA 3B42 data in (a, c) JJA and (d, f) DJF. The grey areas indicate the diurnal harmonics were not statistically significant at the 90% confidence level. (a) Amplitude in IMERG (JJA). (b) Differences of mean precipitation (JJA). (c) Differences of amplitude (JJA). (d) Amplitude in IMERG (DJF). (e) Differences of mean precipitation (DJF). (f) Differences of amplitude (DJF).

amplitude differences. Mean precipitation in the northwest Bay of Bengal was up to 5 mm/d higher in the IMERG data than in the TMPA data, and mean precipitation for the east coast of the Bay of Bengal was up to 5 mm/d lower in the IMERG data than in the TMPA data. This suggests that the differences in the diurnal amplitudes in the Bay of Bengal in JJA in the IMERG and TMPA data were associated with seasonal mean differences in the IMERG and TMPA datasets. The same plots as in Figures 10(a)–10(c) are shown in Figures 10(d)–10(f) but for DJF. The diurnal amplitudes in the Bay of Bengal were much smaller in DJF than JJA, and in most regions no diurnal signals were detected that were statistically significant at the 90% confidence level. For regions with significant diurnal variations in precipitation, the patterns in the differences between the diurnal amplitudes in the IMERG and TMPA datasets were similar to the patterns in the seasonal mean differences in DJF. This suggests that seasonal mean differences caused the differences in diurnal amplitude in both seasons in the Bay of Bengal.

The diurnal amplitudes in the IMERG data, the seasonal mean differences between the IMERG and TMPA data, and differences between the diurnal amplitudes in the IMERG and TMPA data for the west coast of Central America in JJA and DJF, are shown in Figure 11. The seasonal mean diurnal

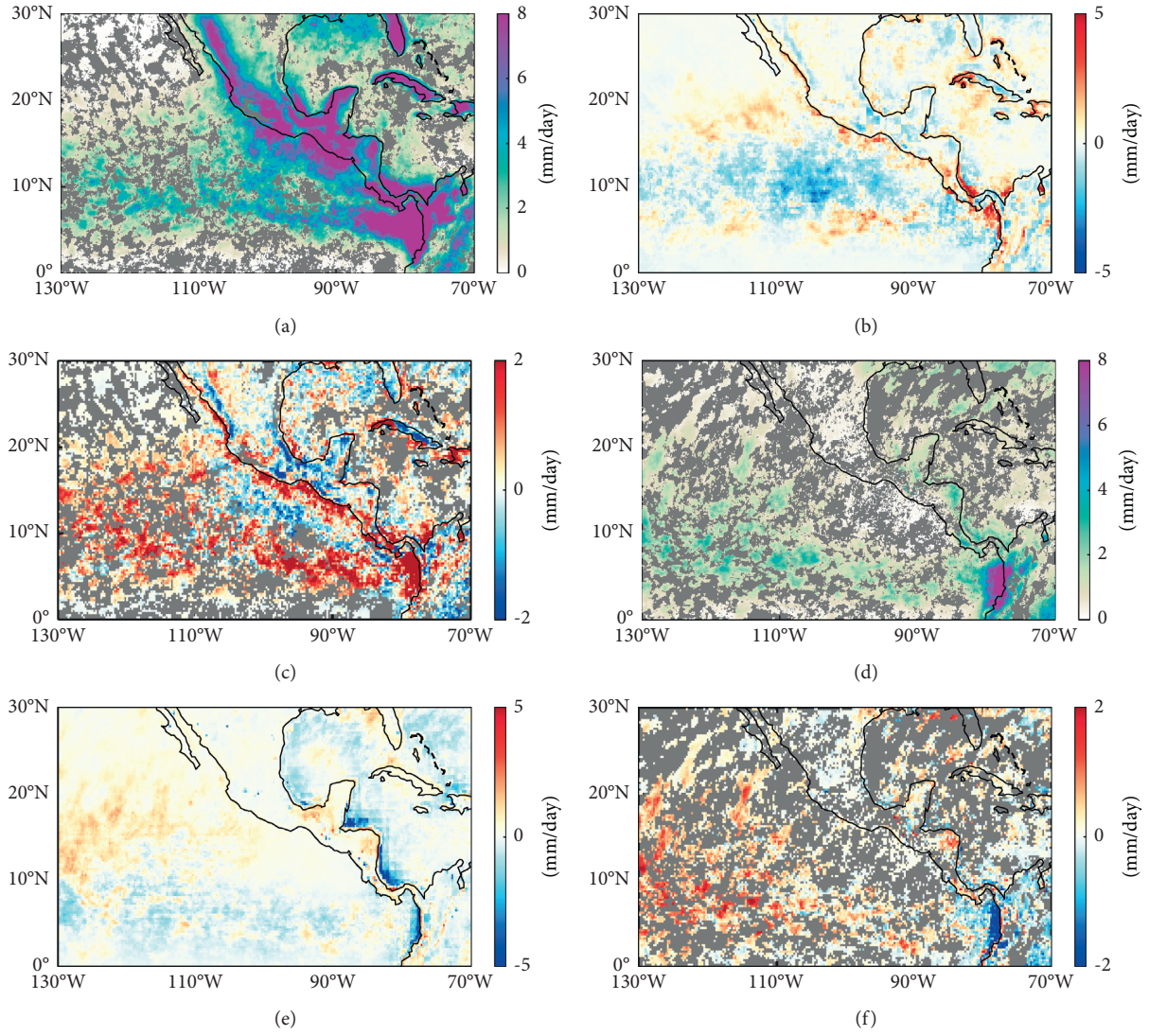

Figure 11: As Figure 10 but for the west coast of Central America. The grey areas indicate the diurnal harmonics were not statistically significant at the 90% confidence level. (a) Amplitude in IMERG (JJA). (b) Differences of mean precipitation (JJA). (c) Differences of amplitude (JJA). (d) Amplitude in IMERG (DJF). (e) Differences of mean precipitation (DJF). (f) Differences of amplitude (DJF).

amplitudes for the west coast of Central America were >8 mm/d (Figure 11(a)). The diurnal amplitudes along the west coast of Central America were as large as the diurnal amplitudes over the continents. The diurnal amplitudes along the west coast of Central America had a consistent pattern of large–small–large in the offshore direction. The differences between the amplitudes along the west coast of Central America in the IMERG and TMPA datasets had a positive–negative–positive pattern in the offshore direction (Figure 11(b)). The positive amplitudes were up to 5 mm/d and the negative amplitudes were up to 2 mm/d. The seasonal mean differences between the IMERG and TMPA data are shown in Figure 11(c). More precipitation along the west coast of Central America was indicated in the IMERG data than in the TMPA data, and less precipitation in most areas off the west coast of Central America is indicated in the IMERG data than in the TMPA data. This suggests that the differences between the diurnal amplitudes along the west coast of Central America in the IMERG and TMPA data in JJA were associated with differences in the seasonal mean diurnal amplitudes. The same plots as in Figures 11(a)–11(c) are shown in Figures 11(d)–11(f) but for DJF. As for the Bay of Bengal, the diurnal amplitudes along the west coast of Central America were much smaller in DJF than in JJA, and in most regions no diurnal signals were detected that were statistically significant at the 90% confidence level. Seasonal mean differences in DJF had a similar range to those seen in JJA, but the differences in diurnal amplitude were smaller in DJF than in JJA. In regions with significant diurnal variations in precipitation, the patterns in the differences in diurnal amplitudes in the IMERG and TMPA datasets were similar to the patterns in the seasonal mean diurnal amplitudes. This indicates that differences between the diurnal amplitudes along the west coast of Central America in the IMERG and TMPA datasets were associated with the seasonal mean diurnal amplitudes in both seasons.

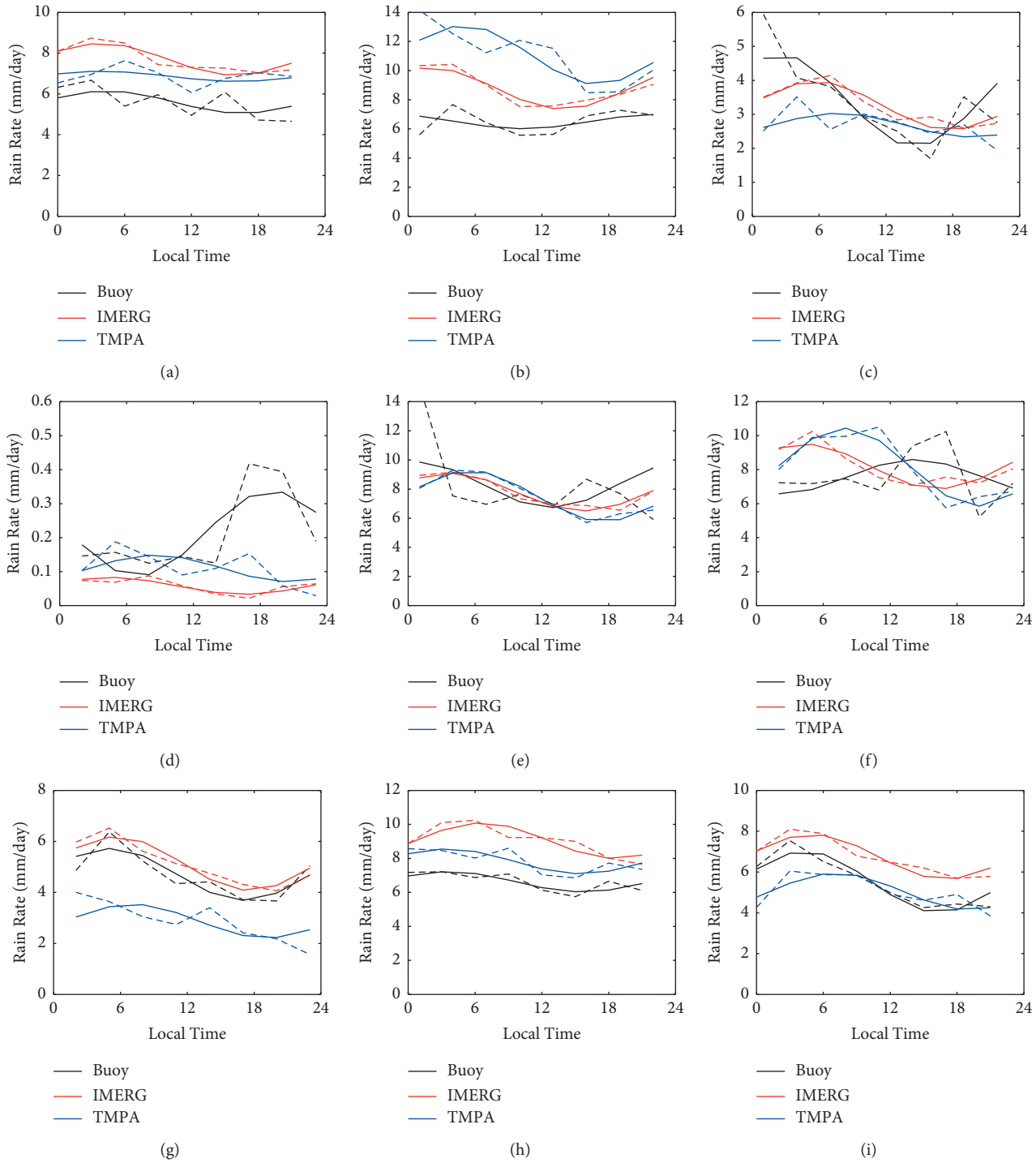

Figure 12: Climatological mean diurnal cycles (dashed lines) and fittings (solid lines) for nine buoys (black lines) and IMERG (red lines) and TMPA (blue lines) at each buoy location. Both IMERG and TMPA data were averaged to $5^\circ \times 5^\circ$ centred on the buoys' positions. (a) Buoy 1. (b) Buoy 2. (c) Buoy 3. (d) Buoy 4. (e) Buoy 5. (f) Buoy 6. (g) Buoy 7. (h) Buoy 8. (i) Buoy 9.

4.4. Comparison of Diurnal Cycles from Satellite Datasets and Ocean Buoys. In the previous sections, we have shown larger diurnal cycle differences between two satellite datasets tended to occur over ocean than over land. In this section, the rain gauge data of ocean buoys were used to validate the diurnal cycles in two satellite datasets. Due to the relative short records of buoy data, the differences in diurnal cycle between satellite datasets and buoys were not examined in four different seasons. The satellite data were area-averaged to reduce the sampling errors [3]. The $5^\circ \times 5^\circ$ area-averaging scale was used for both the IMERG and TMPA data. The climatological mean diurnal cycle for each buoy and the area-averaging IMERG and TMPA data are shown in Figure 12, and the diurnal cycle statistics for each buoy are

Table 1: Mean rain rates, diurnal precipitation amplitudes and peak times for ninxe buoys and for 5° × 5° area-averaged IMERG and TMPA data. The numbers in bold indicate the diurnal signals were detected at the 90% confidence level.

No	Basin	Position	Available days	Mean rain rate (mm/day)			Amplitude (mm/day)			Peaktime (local time)		
				Buoy	IMERG	TMPA	Buoy	IMERG	TMPA	Buoy	IMERG	TMPA
1	Pacific	8°N 137°E	1570	5.595	7.694	6.861	0.550	**0.786**	0.249	4	**4**	4
2		0°N 156°E	1584	6.500	8.786	11.072	0.491	**1.432**	**2.018**	22	**2**	**5**
3	Atlantic	0°N 23°W	449	3.405	3.254	2.680	**1.354**	**0.716**	0.351	**3**	**6**	8
4		10°S 10°W	788	0.212	0.058	0.109	**0.126**	**0.025**	0.039	**19**	**5**	9
5	Indian	4°S 67°E	474	8.291	7.789	7.508	1.568	**1.293**	**1.740**	1	**4**	**6**
6		4°S 80.5°E	692	7.584	8.191	8.146	1.009	**1.321**	**2.294**	14	**4**	**8**
7		12°S 80.5°E	604	4.706	5.131	2.874	**1.022**	**1.055**	0.661	**5**	**6**	7
8		5°S 95°E	1292	6.626	9.045	7.829	**0.597**	**1.044**	**0.734**	**4**	**7**	**3**
9		8°S 95°E	1135	5.517	6.745	5.043	**1.508**	**1.098**	**0.896**	**4**	**5**	**7**

summarized in Table 1. The numbers in bold in Table 1 indicate that the diurnal signals were detected at the 90% confidence level.

All the satellite data and most of the rain gauges detected diurnal signal peaking in the early morning in a statistically significant way. Overall, both satellite datasets showed similar diurnal variations as buoy measurements, except for Buoy 2, Buoy 4, and Buoy 6. Buoy 2 detected an evident semidiurnal cycle; however, semidiurnal cycles were not evident in either satellite datasets. For buoy 4 in the Atlantic Ocean and buoy 6 in the Indian Ocean, a significant peak at about 1400 LST had been found in the precipitation, while a morning peak was shown in both the IMERG and TMPA. The diurnal difference between gauges and satellite datasets could arise because the satellite datasets were 5° × 5° area-averaged. A weaker and shallower afternoon peak over the oceans had been found in the earlier studies using either in situ or satellite measurements [13, 28, 55, 58, 59]. The morning peak was considered as a result of both stratiform and convective from deep clouds while the afternoon peak was only related to convective rainfall from midlevel clouds [58, 60].

5. Discussion

The performances of various versions of the IMERG data have been assessed using ground-based observations (gauges, radars, and buoys) in previous studies. Limited ground observation data are available, particularly over ocean, meaning that the various versions of the IMERG data have not yet been evaluated completely. In comparing the latest IMERG version data with the TMPA data, it has been possible to shed some light on the differences between the IMERG version 06 data and the earlier IMERG version data. The differences between the IMERG version 06 precipitation data and the TMPA precipitation data for the tropical oceans were relatively small. IMERG precipitation prior to version 06 had smaller precipitation than the TMPA in the heavy-rainfall regions in the Tropics. Differences in patterns in the IMERG version 06 precipitation data and TMPA precipitation data over ocean were different from differences in the precipitation data in previous IMERG versions and the TMPA precipitation data, indicating that there were yearly mean differences between the IMERG version 06 data and the earlier IMERG version data. The patterns in the differences between the IMERG version 03 products and TMPA products for the boreal summer and winter over the oceans [16] were very different from the patterns in the differences between the IMERG version 06 products and TMPA products, suggesting that there could be seasonal mean differences between the IMERG version 06 data and the earlier IMERG version data for the oceans. These findings suggested that studies should be very cautious to use different versions of IMERG data for model validations or physical interoperations due to the yearly and seasonal mean differences between the IMERG version 06 data and the earlier IMERG version data.

This study assessed the performances of IMERG and TMPA products at a diurnal scale. IMERG data were found to show great uncertainty in precipitation diurnal amplitude in comparison with in situ rain gauge precipitation data. The diurnal variations were found to be smaller in the IMERG data than the TMPA data over most of the continents and maritime continents in all four seasons. The negative differences between the diurnal amplitudes over land in the IMERG and TMPA data increased with the mean diurnal amplitudes. The diurnal variations over the oceans were found to be larger in the IMERG data than in the TMPA data. The large differences between the diurnal amplitudes over ocean in the IMERG and TMPA datasets may have been caused by large seasonal mean precipitation differences or large diurnal amplitudes. These findings will help to improve IMERG data retrieval at the diurnal scale in the future.

Although fewer differences both in the mean precipitation and the diurnal cycle were shown over land than over ocean between two satellite products, it reveals one of the limitations of this work, namely, that two products share the same gauge calibration over land. The monthly GPCC as the ground validations are more likely to affect the satellite data at longer timescales than a diurnal scale. Over ocean, the atoll and buoy gauge data are only used to validate the algorithms of both the TMPA and the IMERG [10, 12, 26]. It should be noticed and the data should be carefully used in related researches. This study assessed the performances of IMERG and TMPA product from April 2014 to March 2019. The TMPA shifted from Combined to TMI as the calibrator when the PR ended

in October 2014. There is some possibility that there might be a shift in TMPA means when the PR ended, but very likely not in the diurnal cycle.

6. Conclusions

Differences between seasonal and diurnal variations in the IMERG version 06B and TMPA 3B42 version 7 datasets in five years from 1 April 2014 to 31 March 2019 were compared. The overall performances of the IMERG version 06 and TMPA data were comparable. As in earlier IMERG versions, monthly, seasonal, and longer differences between the IMERG version 06 precipitation data and TMPA precipitation data were larger over the oceans than over land because both the IMERG and TMPA products used the same GPCC rain gauge data to adjust the bias over the land. Unlike earlier IMERG versions, the differences between the IMERG version 06 precipitation data and the TMPA precipitation data for the tropical oceans were relatively small, which demonstrates that there are yearly mean differences between the IMERG version 06 data and the earlier IMERG version data. This could be a result of the calibration processes used. The mean differences between the IMERG version 06 precipitation data and the TMPA precipitation data for the tropical oceans were relatively small, but the differences between the IMERG version 06 and TMPA precipitation data for the tropical Pacific were not small for each season. Opposite differences occurred in different seasons, meaning that the 5-year mean differences between the data for the tropical Pacific in the IMERG and TMPA products were not very different.

Unlike for the seasonal mean differences, the differences between the diurnal amplitudes of the precipitation diurnal harmonics over land in the IMERG and TMPA datasets were not small. The diurnal variations were smaller in the IMERG data than the TMPA data for over most of the continents and maritime continents in all four seasons. The differences were largest in the high-rainfall regions in South America and Africa in SON and DJF. The negative differences between the diurnal amplitudes over land in the IMERG and TMPA data increased with the mean diurnal amplitudes. The diurnal variations over ocean were larger in the IMERG data than in the TMPA data. The differences between the phases of the precipitation diurnal harmonics in the IMERG and TMPA datasets varied widely in all four seasons, but the mean phases were almost the same in the IMERG and TMPA datasets over both ocean and land except that the mean maximum time was ~0.5 h earlier in the TMPA data than in the IMERG data in both summer and winter over land, and the mean maximum time was ~0.5 h earlier in the IMERG data than in the TMPA data in autumn over ocean.

The large differences between the diurnal amplitudes over the oceans in the IMERG and TMPA datasets may have been caused by large seasonal mean precipitation differences or large diurnal amplitudes. The sources of error that contributed to the differences in the diurnal precipitation amplitudes in the Bay of Bengal and the west coast of Central America, which had large diurnal ranges and significant differences in diurnal amplitudes, were investigated. The data suggest that seasonal mean differences caused the differences in diurnal amplitudes in the Bay of Bengal, but along the west coast of Central America, differences in diurnal amplitudes were associated with the seasonal mean diurnal amplitudes.

Compared with rain gauge data from ocean buoys, both the IMERG and TMPA had good performances in estimating the diurnal cycle with the maximum in the early morning. However, due to the limited number of buoys to evaluate the performance of two satellite datasets, it is hard to draw conclusions that one dataset has better performance in detecting diurnal variations in precipitation than the other over ocean.

The IMERG product integrates several datasets together, which means that it is not a satellite-observational-only product. The gauge adjustment makes it hard to be validated and adding the model data makes it easy to tune in the algorithm. Although the IMERG V06 product provides a high resolution in estimating the precipitation, there are still limitations for this product.

Data Availability

The IMERG V06 Final data provided by NASA were downloaded from the following website: https://gpm1.gesdisc.eosdis.nasa.gov/data/GPM_L3/GPM_3IMERGHH.06/. The TMPA 3B42 V7 data provided by NASA were downloaded from the following website: https://disc2.gesdisc.eosdis.nasa.gov/data/TRMM_L3/TRMM_3B42.7/.

Conflicts of Interest

The authors declare that there are no conflicts of interest regarding the publication of this paper.

Acknowledgments

Funding for this study was provided by the National Natural Science Foundation of China (Grants 41690121 and 41690120), the Strategic Priority Research Program of the Chinese Academy of Sciences (Grant XDA20060501), and NSFC (41722601).

References

[1] K. E. Trenberth, A. Dai, R. M. Rasmussen, and D. B. Parsons, "The changing character of precipitation," *Bulletin of the American Meteorological Society*, vol. 84, no. 9, pp. 1205–1218, 2003.

[2] K. E. Trenberth, L. Smith, T. Qian, A. Dai, and J. Fasullo, "Estimates of the global water budget and its annual cycle using observational and model data," *Journal of Hydrometeorology*, vol. 8, no. 4, pp. 758–769, 2007.

[3] K. P. Bowman, J. C. Collier, G. R. North, Q. Wu, E. Ha, and J. Hardin, "Diurnal cycle of tropical precipitation in Tropical Rainfall Measuring Mission (TRMM) satellite and ocean buoy rain gauge data," *Journal of Geophysical Research: Atmospheres*, vol. 110, no. D21, 2005.

[4] G. J. Huffman, D. T. Bolvin, E. J. Nelkin et al., "The TRMM Multisatellite Precipitation Analysis (TMPA): quasi-global, multiyear, combined-sensor precipitation estimates at fine

scales," *Journal of Hydrometeorology*, vol. 8, no. 1, pp. 38–55, 2007.

[5] R. J. Joyce, J. E. Janowiak, P. A. Arkin, and P. Xie, "CMORPH: a method that produces global precipitation estimates from passive microwave and infrared data at high spatial and temporal resolution," *Journal of Hydrometeorology*, vol. 5, no. 3, pp. 487–503, 2004.

[6] C. Kidd, D. R. Kniveton, M. C. Todd, and T. J. Bellerby, "Satellite rainfall estimation using combined passive microwave and infrared algorithms," *Journal of Hydrometeorology*, vol. 4, no. 6, pp. 1088–1104, 2003.

[7] G. J. Huffman, R. F. Adler, P. Arkin et al., "The global precipitation climatology project (GPCP) combined precipitation dataset," *Bulletin of the American Meteorological Society*, vol. 78, no. 1, pp. 5–20, 1997.

[8] T. Kubota, S. Shige, H. Hashizume et al., "Global precipitation map using satellite-borne microwave radiometers by the GSMaP project: production and validation," *IEEE Transactions on Geoscience and Remote Sensing*, vol. 45, no. 7, pp. 2259–2275, 2007.

[9] J. E. M. Brown, "An analysis of the performance of hybrid infrared and microwave satellite precipitation algorithms over India and adjacent regions," *Remote Sensing of Environment*, vol. 101, no. 1, pp. 63–81, 2006.

[10] G. J. Huffman, R. F. Adler, D. T. Bolvin, and E. J. Nelkin, "The TRMM multi-satellite precipitation analysis (TMPA)," in *Satellite Rainfall Applications for Surface Hydrology*, pp. 3–22, Springer, Berlin, Germany, 2010.

[11] A. Y. Hou, R. K. Kakar, S. Neeck et al., "The global precipitation measurement mission," *Bulletin of the American Meteorological Society*, vol. 95, no. 5, pp. 701–722, 2014.

[12] G. J. Huffman, D. T. Bolvin, and E. J. Nelkin, "Integrated multi-satellitE retrievals for GPM (IMERG) technical documentation," *NASA/GSFC Code*, vol. 612, no. 47, 2019.

[13] S. Sorooshian, A. AghaKouchak, P. Arkin et al., "Advanced concepts on remote sensing of precipitation at multiple scales," *Bulletin of the American Meteorological Society*, vol. 92, no. 10, pp. 1353–1357, 2011.

[14] F. Satgé, "Benefits of the successive GPM based satellite precipitation estimates IMERG–V03,–V04,–V05 and GSMaP–V06,–V07 over diverse geomorphic and meteorological regions of Pakistan," *Remote Sensing*, vol. 10, no. 9, p. 1373, 2018.

[15] S.-M. Hosseini-Moghari and Q. Tang, "Validation of gpm imerg v05 and v06 precipitation products over Iran," *Journal of Hydrometeorology*, vol. 21, no. 5, pp. 1011–1037, 2020.

[16] Z. Liu, "Comparison of integrated multisatellite retrievals for GPM (IMERG) and TRMM multisatellite precipitation analysis (TMPA) monthly precipitation products: initial results," *Journal of Hydrometeorology*, vol. 17, no. 3, pp. 777–790, 2016.

[17] G. Tang, Y. Ma, D. Long, L. Zhong, and Y. Hong, "Evaluation of GPM Day-1 IMERG and TMPA Version-7 legacy products over Mainland China at multiple spatiotemporal scales," *Journal of hydrology*, vol. 533, pp. 152–167, 2016.

[18] R. Xu, F. Tian, L. Yang, H. Hu, H. Lu, and A. Hou, "Ground validation of GPM IMERG and TRMM 3B42V7 rainfall products over southern Tibetan Plateau based on a high-density rain gauge network," *Journal of Geophysical Research: Atmospheres*, vol. 122, no. 2, pp. 910–924, 2017.

[19] U. V. Murali Krishna, S. K. Das, S. M. Deshpande, S. L. Doiphode, and G. Pandithurai, "The assessment of Global Precipitation Measurement estimates over the Indian subcontinent," *Earth and Space Science*, vol. 4, no. 8, pp. 540–553, 2017.

[20] J. Su, H. Lü, D. Ryu, and Y. Zhu, "The assessment and comparison of TMPA and IMERG products over the major basins of Mainland China," *Earth and Space Science*, vol. 6, no. 12, pp. 2461–2479, 2019.

[21] Q. Wu and Y. Wang, "Comparison of oceanic multisatellite precipitation data from Tropical Rainfall Measurement Mission and Global Precipitation Measurement Mission datasets with rain gauge data from ocean buoys," *Journal of Atmospheric and Oceanic Technology*, vol. 36, no. 5, pp. 903–920, 2019.

[22] R. Li, K. Wang, and D. Qi, "Validating the integrated multisatellite retrievals for global precipitation measurement in terms of diurnal variability with hourly gauge observations collected at 50,000 stations in China," *Journal of Geophysical Research: Atmospheres*, vol. 123, no. 18, p. 10, 2018.

[23] Y. Mayor, I. Tereshchenko, M. Fonseca-Hernández, D. Pantoja, and J. Montes, "Evaluation of error in IMERG precipitation estimates under different topographic conditions and temporal scales over Mexico," *Remote Sensing*, vol. 9, no. 5, p. 503, 2017.

[24] R. Oliveira, V. Maggioni, D. Vila, and C. Morales, "Characteristics and diurnal cycle of GPM rainfall estimates over the central Amazon region," *Remote Sensing*, vol. 8, no. 7, p. 544, 2016.

[25] O. Sungmin and P. E. Kirstetter, "Evaluation of diurnal variation of GPM IMERG-derived summer precipitation over the contiguous US using MRMS data," *Quarterly Journal of the Royal Meteorological Society*, vol. 144, pp. 270–281, 2018.

[26] G. J. Huffman, "Algorithm theoretical basis document (ATBD) version 06," *NASA Global Precipitation Measurement (GPM) Integrated Multi-Satellite Retrievals for GPM (IMERG), NASA*, 2019, https://pmm.nasa.gov/data-access/downloads/gpm.

[27] J. Tan, G. J. Huffman, D. T. Bolvin, and E. J. Nelkin, "Diurnal cycle of IMERG V06 precipitation," *Geophysical Research Letters*, vol. 46, no. 22, pp. 13584–13592, 2019.

[28] S. W. Nesbitt and E. J. Zipser, "The diurnal cycle of rainfall and convective intensity according to three years of TRMM measurements," *Journal of Climate*, vol. 16, no. 10, pp. 1456–1475, 2003.

[29] S. Sen Roy and R. C. Balling Jr., "Diurnal variations in summer season precipitation in India," *International Journal of Climatology*, vol. 27, no. 7, pp. 969–976, 2007.

[30] S. Yang and E. A. Smith, "Mechanisms for diurnal variability of global tropical rainfall observed from TRMM," *Journal of Climate*, vol. 19, no. 20, pp. 5190–5226, 2006.

[31] S. Sahany, V. Venugopal, and R. S. Nanjundiah, "Diurnal-scale signatures of monsoon rainfall over the Indian region from TRMM satellite observations," *Journal of Geophysical Research: Atmospheres*, vol. 115, no. D2, 2010.

[32] M. Biasutti, S. E. Yuter, C. D. Burleyson, and A. H. Sobel, "Very high resolution rainfall patterns measured by TRMM precipitation radar: seasonal and diurnal cycles," *Climate Dynamics*, vol. 39, no. 1, pp. 239–258, 2012.

[33] A. Dai, X. Lin, and K.-L. Hsu, "The frequency, intensity, and diurnal cycle of precipitation in surface and satellite observations over low-and mid-latitudes," *Climate Dynamics*, vol. 29, no. 7-8, pp. 727–744, 2007.

[34] B. Wang, H.-J. Kim, K. Kikuchi, and A. Kitoh, "Diagnostic metrics for evaluation of annual and diurnal cycles," *Climate Dynamics*, vol. 37, no. 5, pp. 941–955, 2011.

[35] H. Chen, W. Yuan, J. Li, and R. Yu, "A possible cause for different diurnal variations of warm season rainfall as shown in station observations and TRMM 3B42 data over the southeastern Tibetan Plateau," *Advances in Atmospheric Sciences*, vol. 29, no. 1, pp. 193–200, 2012.

[36] S. Prakash, A. K. Mitra, E. N. Rajagopal, and D. S. Pai, "Assessment of TRMM-based TMPA-3B42 and GSMaP precipitation products over India for the peak southwest monsoon season," *International Journal of Climatology*, vol. 36, no. 4, pp. 1614–1631, 2016.

[37] J. A. Giles, R. C. Ruscica, and C. G. Menéndez, "The diurnal cycle of precipitation over South America represented by five gridded datasets," *International Journal of Climatology*, vol. 40, no. 2, pp. 668–686, 2020.

[38] L. Y. Worku, A. Mekonnen, and C. J. Schreck III, "Diurnal cycle of rainfall and convection over the Maritime Continent using TRMM and ISCCP," *International Journal of Climatology*, vol. 39, no. 13, pp. 5191–5200, 2019.

[39] A. R. As-syakur, "Analysis of spatial and seasonal differences in the diurnal rainfall cycle over sumatera revealed by 17-year TRMM 3B42 dataset," *SOLA*, vol. 15, 2019.

[40] A. K. Dezfuli, C. M. Ichoku, G. J. Huffman et al., "Validation of IMERG precipitation in Africa," *Journal of Hydrometeorology*, vol. 18, no. 10, pp. 2817–2825, 2017.

[41] S. Prakash, M. R. Kumar, S. Mathew, and R. Venkatesan, "How accurate are satellite estimates of precipitation over the north Indian Ocean?" *Theoretical and Applied Climatology*, vol. 134, no. 1, pp. 467–475, 2018.

[42] J. Tan and G. J. Huffman, *Computing Morphing Vectors for Version 06 IMERG*, NASA/GSFC, Greenbelt, MD, USA, 2019.

[43] J. Tan, G. J. Huffman, D. T. Bolvin, and E. J. Nelkin, "Imerg V06: changes to the morphing algorithm," *Journal of Atmospheric and Oceanic Technology*, vol. 36, no. 12, pp. 2471–2482, 2019.

[44] M. J. McPhaden, "The global tropical moored buoy array," *Proceedings of OceanObs*, vol. 9, pp. 668–682, 2010.

[45] S. P. Hayes, L. J. Mangum, J. Picaut, and A. Sumi, "TOGA-TAO: a moored array for real-time measurements in the tropical Pacific Ocean," *Bulletin of the American Meteorological Society*, vol. 72, no. 3, pp. 339–347, 1991.

[46] M. J. McPhaden, "The tropical ocean-global atmosphere observing system: a decade of progress," *Journal of Geophysical Research: Oceans*, vol. 103, no. C7, pp. 14169–14240, 1998.

[47] Y. L. Serra, P. A'Hearn, H. P. Freitag, and M. J. McPhaden, "ATLAS self-siphoning rain gauge error estimates," *Journal of Atmospheric and Oceanic Technology*, vol. 18, no. 12, pp. 1989–2002, 2001.

[48] J. Servain, "A pilot research moored array in the tropical Atlantic (PIRATA)," *Bulletin of the American Meteorological Society*, vol. 79, no. 10, pp. 2019–2032, 1998.

[49] B. Bourles, "The PIRATA program: history, accomplishments, and future directions," *Bulletin of the American Meteorological Society*, vol. 89, no. 8, pp. 1111–1126, 2008.

[50] M. J. McPhaden, "RAMA: the research moored array for african–asian–Australian monsoon analysis and prediction," *Bulletin of the American Meteorological Society*, vol. 90, no. 4, pp. 459–480, 2009.

[51] J. C. Collier and K. P. Bowman, "Diurnal cycle of tropical precipitation in a general circulation model," *Journal of Geophysical Research: Atmospheres*, vol. 109, Article ID D17105, 2004.

[52] A. Dai, "Global precipitation and thunderstorm frequencies. Part II: diurnal variations," *Journal of Climate*, vol. 14, no. 6, pp. 1112–1128, 2001.

[53] X. He, "The diurnal cycle of precipitation in regional spectral model simulations over West Africa: sensitivities to resolution and cumulus schemes," *Weather and Forecasting*, vol. 30, no. 2, pp. 424–445, 2015.

[54] T. W. Anderson, *The Statistical Analysis of Time Series*, p. 704, John Wiley, Hoboken, NJ, USA., 1971.

[55] G.-Y. Yang and J. Slingo, "The diurnal cycle in the tropics," *Monthly Weather Review*, vol. 129, no. 4, pp. 784–801, 2001.

[56] R. Carbone and J. Tuttle, "Rainfall occurrence in the US warm season: the diurnal cycle," *Journal of Climate*, vol. 21, no. 16, pp. 4132–4146, 2008.

[57] C. Junquas, "Understanding the influence of orography on the precipitation diurnal cycle and the associated atmospheric processes in the central Andes," *Climate Dynamics*, vol. 50, no. 11, pp. 3995–4017, 2018.

[58] C. Sui, K. Lau, Y. Takayabu, and D. Short, "Diurnal variations in tropical oceanic cumulus convection during TOGA COARE," *Journal of the Atmospheric Sciences*, vol. 54, no. 5, pp. 639–655, 1997.

[59] Y. L. Serra and M. J. McPhaden, "In situ observations of diurnal variability in rainfall over the tropical Pacific and Atlantic Oceans," *Journal of Climate*, vol. 17, no. 18, pp. 3496–3509, 2004.

[60] J. E. Janowiak, P. A. Arkin, and M. Morrissey, "An examination of the diurnal cycle in oceanic tropical rainfall using satellite and in situ data," *Monthly Weather Review*, vol. 122, no. 10, pp. 2296–2311, 1994.